


Institut Polytechnique de Grenoble

Master 2 Reserch Thesis in Automatic Control

Particle source identification in the plasma edge in Tore Supra tokamak

Author:
Enrique SANTIAGO

Supervisors:
Emmanuel WITRANT
[UJF/GIPSA-lab]
Marc GONICHE
[CEA-IRFM]

Abstract: In this research project we aim to develop a new identification technique to study the plasma phenomena taking place in the so-called *scrape-off layer* (SOL) and its correlation with the current drive *lower hybrid* antenna in the experimental nuclear fusion tokamak reactor *Tore Supra*. A deeper knowledge of the plasma behavior in this region would contribute to the achievement of steady-state controlled thermonuclear fusion for power generation.

Resumé: Dans ce projet de recherche nous avons comme objectif le développement d'une nouvelle technique d'identification pour l'étude du comportement du plasma dans la région appellé *scrape-off layer* (SOL) ainsi que sa relation avec la source de courant induite par l'*antenne LH* dans le réacteur tokamak expérimental de fusion nuclaire *Tore Supra*. Une connaissance plus profonde de ces phénoménes contribuerait à réussir la fusion thermonucléaire contrôlée de longue durée pour la generation d'énergie.

February - June, 2010

General purpose of the project

Nuclear fusion power is one of the main hopes with regard to meet world's future energy needs with responsibility and sustainability. But the high complexity degree for the physics that governs this potential energy source makes necessary the use of advanced analysis and identification methods to understand and then to control thermonuclear fusion power.

In this project, control theory and plasma physics merge with the aim to show one of the possible applications of the new identification methods from control theory and with the hope to make a small but dedicated contribution towards the achievement of controlled thermonuclear fusion.

Once the project background and the necessary concepts are introduced, the project objective will be stated in section 2.3. Essentially, as it yields from this thesis title, what we aim to do is to identify an input term (the so-called source term) in the equations modeling the fusion plasma behavior in a determined region (the scrape-off layer).

This project has been possible thanks to the guidance and transferred knowledge from the two persons that tutored me in this internship: Mr. Emmanuel Witrant (GIPSA-lab) and Mr. Marc Goniche (IRFM).

In this thesis, the project background, the research work and the main results obtained from this project are presented. Though this thesis can be integrally comprehended for itself, extended appendices explaining in detail some developments, procedures and results obtained during the internship have been included in order to offer the reader a deeper study of the project.

Acknowledgements

In first place I would like to thank Emmanuel Witrant, from the GIPSA-lab, and Marc Goniche, from the CEA-IRFM, for guiding me through this internship.
Emmanuel Witrant proposed me this project as final master thesis. He received me in the GIPSA-lab and he assisted me during the whole internship with his knowledge in automatic control.
Marc Goniche received me in the CEA-IRFM. He instructed me in the basis of nuclear fusion physics and helped me to understand the theoretical aspects of the project.
I would also like to thank both institutions, the GIPSA-lab and the IRFM and their respective teams for providing me with the means to carry out this project.

I am also grateful to the INPG $ENSE^3$ school for receiving me during this year and for enriching this international experience with the transferred knowledge and values.

Finally, I want to thank my workmates at both institutions for making this internship even more pleasant and for helping me with their ideas.

Contents

Chapter 1

Introduction: Towards nuclear fusion power generation

In this chapter, a general introduction to the project background is carried out. At first, the appeals of thermonuclear controlled fusion as a possible solution to the future energy supply problematic are enumerated. Then, the fundamentals of thermonuclear controlled fusion are exposed and finally, the nuclear "tokamaks" reactors basis are exposed.

1.1 Nuclear fusion power: Great expectations

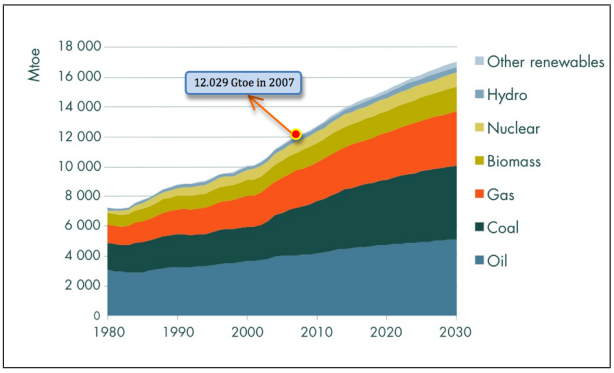

Figure 1.1: Global energy demand estimation. Source: IEA

Estimations in [1] and [2] predicts a marked increase in the global energy demand for the next years. In figure 1.1 it can be observed that even if an increasing relevance for the rest of the fuels is expected, fossil fuels will be keeping the main role in the long term energy supply framework. But, is it possible to expect a substantial change in this situation?.

Since the second half of the past century, a growing number of researchers has been working in a extraordinary quest: Reproducing in Earth the phenomenon fueling the stars. This phenomenon is the nuclear fusion, and it could be the affirmative answer to the previous question.

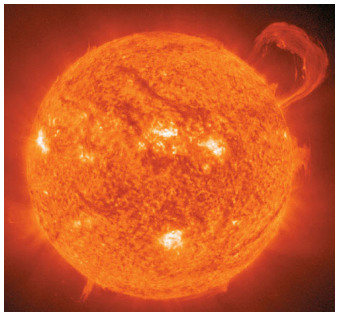

Figure 1.2: Nuclear fusion fuels the stars

Once it will be controlled, thermonuclear fusion power could be a solution for the future global energy needs, since it could provide an efficient, sustainable and environmentally responsible power supply. The main advantages of thermonuclear power are:

- Almost limitless fuel : Water and lithium are the basic fuels for fusion. These two substances are abundant in the Earth surface. From water, deuterium is obtained ($0.033 g_{H^2}/l_{H_2O}$), and tritium, even though cannot be found in nature, can be obtained from lithium in the reactor (when neutrons impact the lithium blanket, tritium is produced). In addition, its fuel consumption will be extremely low. A 1 gigawatt electric fusion power plant would consume 100 kg of deuterium and three tons of lithium a year. In the same conditions, a coal-fired power station would consume 1.5 million tons of coal.
- Inherent safety: Thermonuclear fusion can only be achieved in very specific conditions. In fact, this is the main drawback against fusion power, but this is also an advantage, since the odds of a runaway situation are negligible. In addition, water and lithium (fusion raw fuels) are not radioactive. In the other hand, tritium is mildly radioactive, but since it will be produced in the reactor itself, the radioactive risk can be considered as very low.
- Environmentally responsible: No greenhouse gasses will be emitted to the atmosphere in fusion power, and with the appropriate choice of plasma facing materials, the radioactive residuals from a fusion plant (generated because of the interaction between neutrons and the plasma facing elements) would be considered safe before 100 years.

These advantages make of fusion power a very attractive solution for the future energy supply.

1.2 Thermonuclear controlled fusion

In 1905, the mass-energy equivalence equation ($E = mc^2$) appears for the first time in the "Theory of special relativity", published by Albert Einstein (1879-1955). From this equation it yields that the conversion of a small quantity of mass can throw a large amount of energy. Three decades later, this equation would appear once again in Bethe's "Theory of stellar nucleosynthesis" (Hans Bethe, 1939), applied to the energy generation by fusion reactions in the stars. The nuclear fusion research had started.

Although the first major steps in fusion research were dedicated to weapon design, since the beginning of the second half of the century nuclear fusion research with power generation purposes has occupied a relevant place.

In this section, a brief introduction to the principles of nuclear fusion is done. Also a review of the state of the art for human induced fusion reactions (especially under magnetic confinement) is made.

1.2.1 The fusion reaction

When two light nuclei fuse together to form a heavier one, the mass of the nucleons in the new nuclei is slightly smaller than the nucleons in its separated state. This mass difference can be explained by the fundamental nuclear forces that held the nucleons together.

The energy cost to separate two nucleons is called the binding energy (fig.1.3), and its relation with the mass ratio (free nucleon/combined nucleon) is expressed by $E = mc^2$. Iron is the element with the the higher binding energy (8.5 MeV per nucleon), and thus, the smaller mass ratio (0.992). This ratio is always very small, but since it is multiplied by c^2, the amount of energy involved is very high.

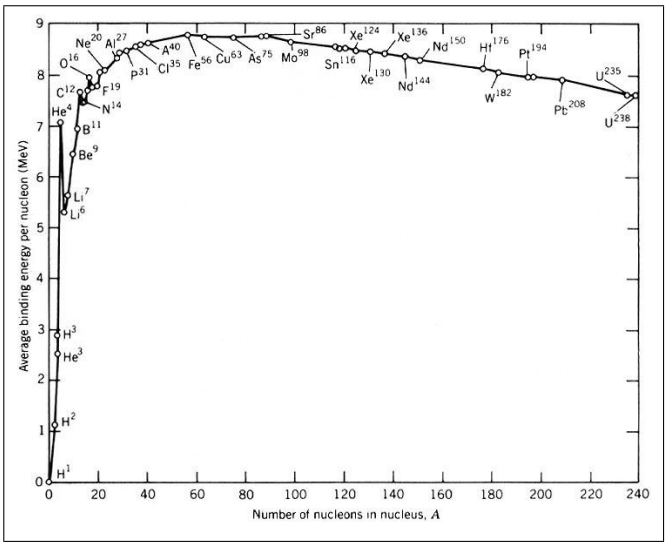

Figure 1.3: Binding energies. Source: European Nuclear S.

Then, if two light nuclei (from the left part of the diagram in figure 1.3) fuse to give a heavier one, a large amount of energy will be released. In figure 1.4, the deuterium-tritium nuclear reaction is schematized.

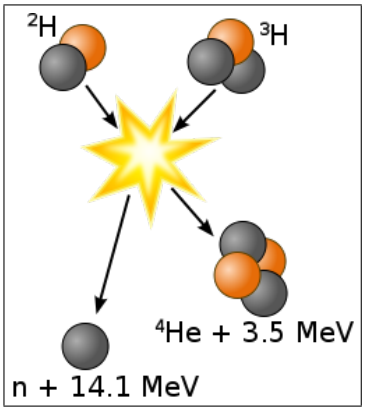

Figure 1.4: Deuterium-Tritium fusion reaction

When the deuterium and tritium nuclei are close enough, nuclear interactions (characterized by very high strength and very short range) appear, and the two nuclei merge to produce a helium nucleus (composed by two protons and two neutrons), a neutron, and 17,6 MeV of kinetic energy (14,1 for He and 3,5 for the neutron). This energy is larger than the energy needed to separate the nucleons in the initial nuclei.

But the main obstacle for the nuclear fusion to happen is that, even though nuclear interaction is the strongest existing fundamental interaction (2 orders of magnitude larger than the electromagnetic interaction and 38 orders of magnitude larger than the gravitational force), its range its very limited ($10^{-15}m \approx$ medium nucleus diameter). The involved nuclei must be very near, and for that, the electromagnetic repulsion forces (both nuclei have positive charge) must be overcome. The theoretical magnitude of this force can be calculated with Coulomb's law. As an example, the theoretical needed energy to approach the deuterium and tritium nuclei in the reaction shown in figure 1.4 to 5 femtometer will be estimated:

$$E = \int_{\infty}^{5\cdot10^{-15}} Fdr = \int_{\infty}^{5\cdot10^{-15}} k\frac{q\cdot q}{r^2}\cdot dr = -k\frac{q\cdot q}{r}|_{\infty}^{5\cdot10^{-15}} =$$

$$= -9\cdot10^{9}\frac{Nm^2}{C^2}\frac{(1.602\cdot10^{-19})^2C^2}{5\cdot10^{-15}m} = 4.6\cdot10^{-14}J = 288.3keV \approx 3.3\cdot10^{9}K \qquad (1.1)$$

Then, Coulomb's law estimates that tritium and deuterium nuclei should be heated up to 3 billion Kelvin to achieve nuclear fusion. If this estimation was right, nuclear fusion wouldn't be possible to achieve on Earth. Fortunately, due to the fast ions fraction and the tunnel effect, this value lowers in practice down to 150 million Kelvin for the D-T reaction. This temperature, though extremely high (the sun temperature is estimated to be 15 million Kelvin), can be reached nowadays, making it possible to achieve induced thermonuclear fusion. At this temperature, the gas will be in plasma state, i.e. electrons and ions will be completely separated and thus, its conductivity will be very high (plasma resistivity at 1 keV $\approx$ Cu resistivity).

It must be noticed that the ideal fusion reaction would be the deuterium-deuterium one, since deuterium abounds in nature ($33g/l_{H_2O}$) and it's non radioactive (unlike tritium), but at the previous temperature, D-D reaction capacity is very weak. That is the main reason why the forecasted nuclear reaction for power production plants is the D-T reaction. In the other hand, D-D is the most studied reaction in fusion research experiments (since it doesn't entail the radioactive risk and its handling is easier). The obtained research results are extrapolated to the D-T case. Nevertheless, D-T has been already used in some of the fusion experiments (JET 1991, TFTR 1994).

As it has been previously stated, the plasma must be heated up to extremely high temperatures (around 150 million degrees). At this temperature, the ions have a very high thermal energy, and the plasma tends to expand and to cool down. This is the main difficulty for thermonuclear controlled fusion: the plasma must be isolated and confined at a very high temperature for a sufficient long time for the fusion reactions to take place and release the energy enough to compensate for energy losses and maintain the plasma at that temperature.

1.2.2 Reproducing fusion on Earth: The confinement problem

From the energy balance in fusion plasmas, we can take out the following energy equation:

$$\frac{dW}{dt} = P_{alpha} + P_{external} + P_{losses} \tag{1.2}$$

where $\frac{dW}{dt}$ is the energy gained by the plasma ($\Rightarrow 0$ in steady state), P_{alpha} is the power transmitted by the α particles (helium ions) to the plasma itself, $P_{external}$ is the additional power (from external heating) given to the plasma and P_{losses} stands for the energy losses in plasma due to radiation and imperfect confinement.

The energy transmitted to the plasma itself, P_{alpha}, represents about the 20% of the total energy in the reaction. The remaining energy leaks from the plasma transported by the neutrons and it represents the maximum theoretical energy that can be retrieved from the fusion reactions, P_{fus}. (We can also say that $P_{plasma} = P_{fus} + P_{alpha}$).

Lets now introduce some key definitions to understand the problem:

- **Confinement time**, t_E. Is the time that takes to the plasma to "empty" its energy when no externals sources are supplied.
- **Amplification factor**, $Q = P_{plasma}/P_{external}$. Is the ratio between the total fusion plasma power and the external power that must be applied to it.
- Q=1 is what we call the **break-even point**, and at that point the power in the plasma equals the power supplied by the external heat sources (i.e. $P_{fus} = P_{external}$).

- **Ignition point**. Is the situation given when $P_{fus} = P_{losses}$. At that moment, the plasma would be self-maintained (theoretically $P_{external} = 0$ and $Q = \infty$).

In practice, the needed Q value for power generation is expected to be around $Q = 30$.

To achieve fusion power generation, a sufficient dens (n) and hot plasma (T) has to be confined and self-maintained at least a time t_E. The Lawson criterion gives the necessary temperature T to achieve the break-even point for a plasma given it's nt_E product (Lawson parameter, L). The modified Lawson curve can be seen in figure 1.5. This curve is slightly moved upwards with respect to the Lawson curve, and it represents the ignition conditions instead of break-even conditions.

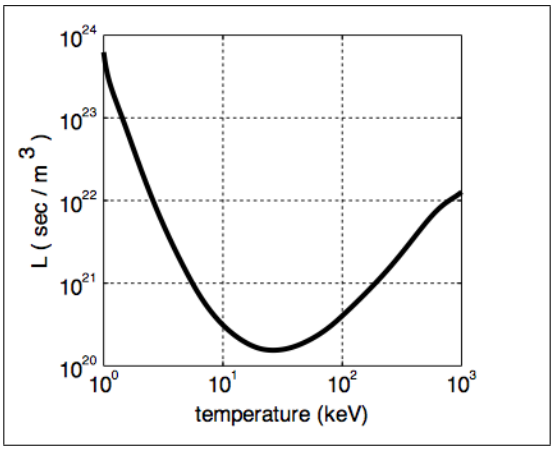

Figure 1.5: Lawson criterion curve. Source: Wikipedia. Verified in [5]

Thus, the confinement problem consists, in short, in obtaining the necessary nT product for a given temperature (we must remember that, up to now, maximum achieved temperature is around 150 million K $\approx$ 15 keV). Nowadays, there are two main investigation lines for this goal: Inertial confinement fusion and magnetic confinement fusion.

- The strategy in **inertial confinement fusion** consists in heating and compressing a small fuel pellet (normally composed by D-T) using high energy beans of particles or laser light. With this mechanism, a very high density (around $10^{32} particles/m^3$, i.e. 10^6 times the air density) is obtained at the fusion temperature (around 150 million degrees) during a very short confinement time t_E (around 10^{-10}s).

$$T \approx 15keV \rightarrow n \uparrow\uparrow t_E \downarrow\downarrow$$

- In the other hand, **magnetic confinement fusion** aims to obtain a big volume of low density plasma (around $10^{20} particles/m^3$, much lower than the density of air) at the fusion temperature during a relatively long time (order of seconds). The two main devices under research at present to induce magnetic confinement fusion are stellarators and tokamaks.

$$T \approx 15keV \rightarrow n \downarrow\downarrow t_E \uparrow\uparrow$$

Our project will be centered in magnetic confinement fusion in tokamaks.

1.3 Magnetic confinement devices: The tokamaks

In this section, the fundamentals of tokamaks operation are expounded.

1.3.1 Tokamaks: past, present and future

In 1946, a fusion reactor was already proposed by Thomson and Blackman. Though this first device was much smaller than the actual tokamaks, it already featured a toroidal vacuum chamber and radio-frequency current drives, two of the main features of modern tokamaks.

In 1956, soviet physicists Igor Tamm and Andrei Sakharov, from the Moscow University, revealed to the occidental world for the first time a nuclear fusion reactor in *tokamak* configuration (toroidal chamber with magnetic coils).

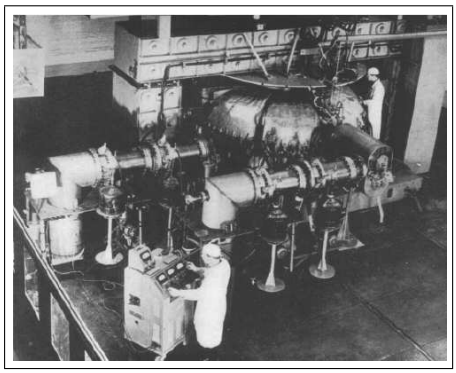

Figure 1.6: T3 tokamak. Source: tokamak.info

In 1968, the T3 tokamak (Moscow) produced far better results than the previous magnetic devices: electronic temperature up to 1 keV, $4 \cdot 10^{19} m^{-3}$ density and a confinement time equal to 7 ms. This results were obtained with a relative small tokamak (12 cm of minor plasma radius).

If, as it was expected, the confinement time was related to diffusive mechanisms, this time would be proportional to the square of the tokamak dimension. This fact was experimentally proved fifteen years later, with the construction of the large modern tokamaks (fig. 1.7): JET (UK, 1983 - still operating) and Tore Supra (France, 1988- still operating). This last one is the first large tokamak build with superconducting toroidal coils, which has allowed to achieve the longest plasma discharge (not to mistake for the confinement time, t_E) at high temperature : 6 minutes and 30 seconds at $T_e \approx 5$ keV in December 2003.

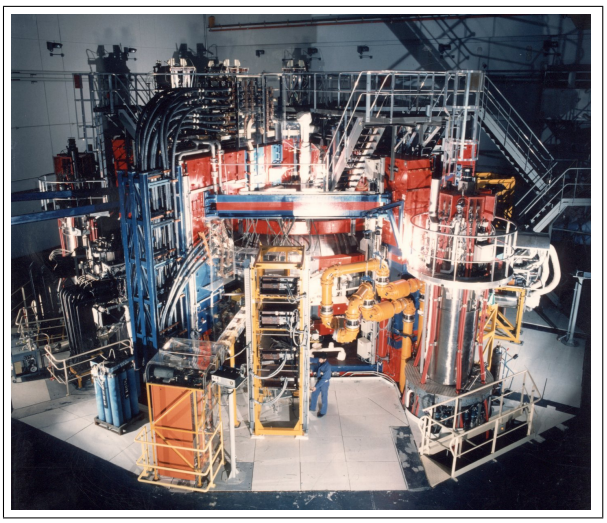

(a) Tore Supra tokamak

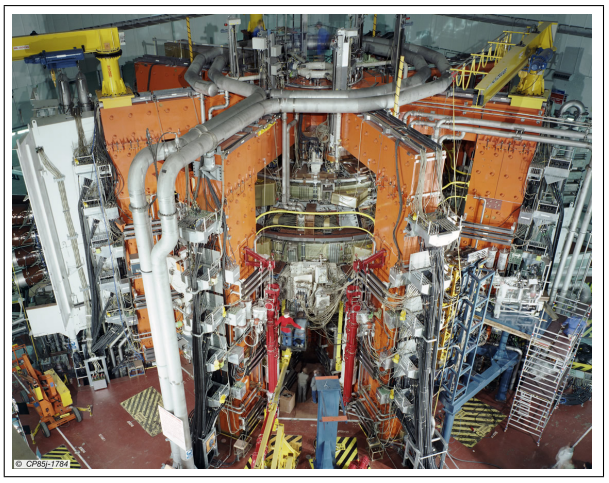

(b) JET tokamak

Figure 1.7: World leading tokamaks TS and JET. Source: TS and JET sites

Nowadays, after 40 years of considerable progress, the goal is to finally prove the viability of controlled fusion for energy production. This challenge goes to the ITER project. The ITER tokamak, now under construction in the Cadarache site, is an international joint project, whose partners are Europe, China, Japan, India, South Korea, Russia and the USA.

This experimental reactor, much larger than the present TS and JET (see figure 1.8 and appendix C), is expected to achieve an amplification factor Q=10 and 400 MW of power generation during 400 s pulse duration (see appendix C). ITER shall be the last step towards the first power fusion plant prototype (DEMO). Its first operation is forecasted for year 2018.

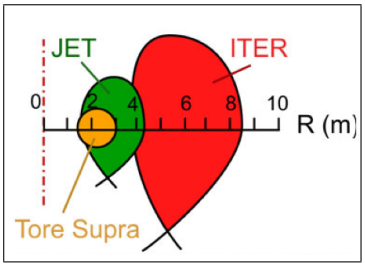

Figure 1.8: TS, JET and ITER major and minor radius. Source: Futura Sciences

1.3.2 Tokamak fundamentals and Tore Supra tokamak

Next, a brief description of the basic working and the different components of a tokamak is be done. For further details about TS tokamak features, see appendix C.

Tokamaks are equipped with a ***vacuum toroidal chamber*** in which the fusion fuel (deuterium in most experimental tokamaks and tritium-deuterium for future power plants) is introduced and turned into plasma heated up to a temperature higher than 100 million degrees so that fusion reactions can take place in it.

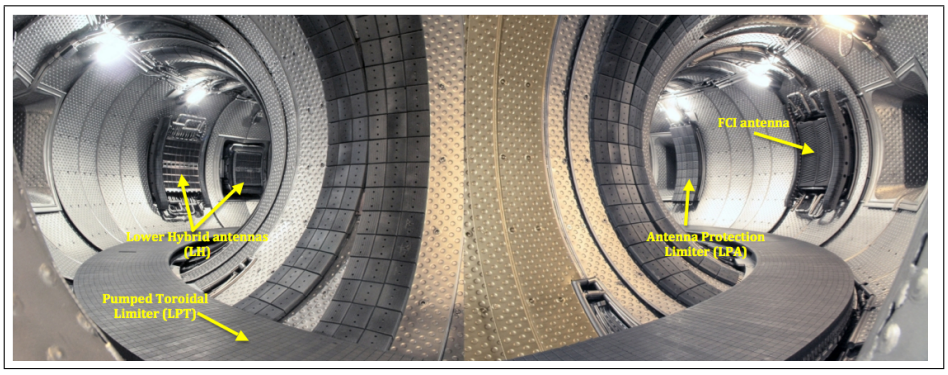

Figure 1.9: Tore Supra vacuum chamber and face to plasma components (Limiters, antennas and rings).

To confine and heat the plasma, tokamaks dispose of three ***sets of magnetic coils*** (fig. 1.10a):

- *Central coils*: These coils are situated in the axis of the tokamak. They work as the primary circuit of a transformer, i.e. when a time variant current is applied to the central coils, a time variant magnetic field is generated. This field induces in the plasma itself (that would work as the secondary circuit of the transformer) a toroidal current of the order of MA with two important missions: To induce the poloidal component of the helicoidal magnetic field (fig. 1.10b) and to heat the plasma by the Joule effect. This effect is called "ohmic heating", and it's an effective way of heating the plasma. But the main problem for the ohmic heating is that its efficiency decreases with the rising of the temperature. In fact, the maximum temperature that the ohmic

heating can achieve is around 20 million degrees in TS (depends on the density). Then other heating mechanisms are needed. That is what we call "external heating".

- *Toroidal coils*: The toroidal coils are circular shaped coils (D shaped in JET and ITER) uniformly distributed around the toroidal chamber (in TS there are 18 toroidal coils that can generate a 4.5 T toroidal field in the middle of the chamber). These coils aim to generate the toroidal component (stronger than the poloidal one) of the helicoidal field confining the plasma (fig. 1.10b).
- *Poloidal coils*: Circular coils contained in parallel planes perpendicular to the tokamak axis. These coils are the ones in charge of placing and controlling the plasma shape. They also contribute to the heating process at the beginning of the plasma discharge. In TS there are 6 poloidal coils.

  In the case of TS tokamak, the toroidal coils are built using superconducting materials actively cooled with helium. This two facts allow to TS tokamak to perform long term plasma discharges.

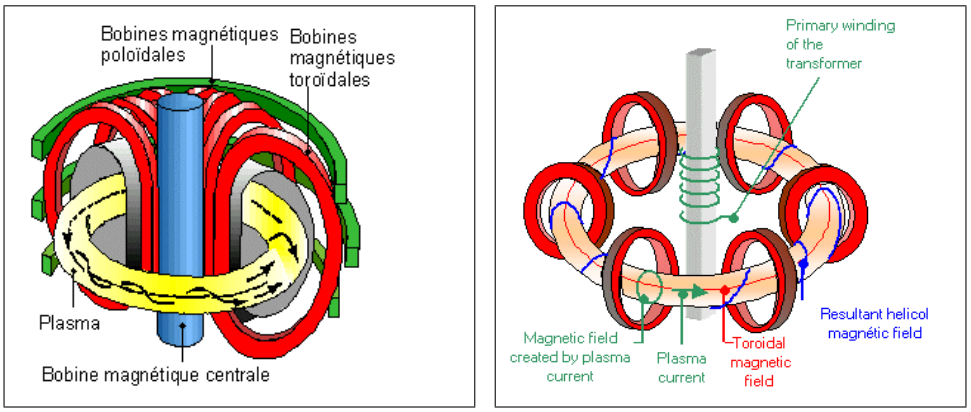

(a) Magnetic coils representation in TS (b) Magnetic fields representation in TS

Figure 1.10: Coils and Fields in TS tokamak. Source: IRFM-TS

Ohmic heating is not enough to achieve the needed temperature in plasma. For further heating, external equipment is needed. This ***external heating***, though less efficient than the ohmic heating, is needed to rise the temperature in the middle of the plasma up to 1.5 keV in TS.

There are two main external mechanisms to heat the plasma:

- Heating by a high energy *neutral particles* beam. The plasma temperature is increased due to the collisions between the plasma particles and the highly energetic injected neutral particles. In the JET tokamak, up to 30 MW power can be transmitted to the plasma using this heating technique. TS is not equipped with this heating method.
- Heating by *radio frequency waves*. Plasma particles gain energy from the coupled electromagnetic waves. This energy may be transmitted by cyclotronic absorption, (the wave is coupled at the resonating rotation frequency of the particles around the field lines) or by the Landau effect (the wave is coupled in resonance frequency with a determined population of particles so that the propagation speed for the wave is close to the particles velocity). The electromagnetic waves are launched from the plasma periphery by antennas powered by generators located away from the tokamak. In TS there are three different kinds of radio frequency heating antennas: the

Ion-Cyclotron Radio Frequency antenna (ICRF) working at 30-80 MHz, the Electron Cyclotron Radio Frequency antenna (ICRH) at 118 GHz (both of them based on cyclotronic absorption) and the Lower Hybrid Radio Frequency antenna (LH) at 3.7 GHz (based on the Landau effect). In TS this last mechanism (LH) injects up to 4 MW power.

The ***LH antenna*** (fig. 1.9) does not only heat the plasma but also induces electric current in it. In fact, this is its main function, and that's why it is considered as a current drive (as the central solenoid). But unlike the other current drives, since the LH antenna working is non inductive, it allows long term plasma discharges.

The ***Pumped Toroidal Limiter (LPT)*** is a toroidal ring built with stainless steel covered with carbon fiber plates that are able to support very high thermic loads. It is located at the bottom of the vacuum chamber (fig. 1.9) and its main function is to exhaust the power from the plasma and to pump a small fraction of the neutralized deuterium particles leaving the plasma (recycling).

In the plasma, the last surface of the helicoidal magnetic field is what we call the *last closed magnetic surface (LCMS)* or separatrix, and it's considered as the limit of the confined plasma region. From the LCMS to the wall of the chamber, the plasma is no longer confined, i.e. the field lines are no longer closed in themselves (as it occurs inside the confined plasma), so the particles following these lines end up crashing against the limiter or the chamber wall. This region of non-confined plasma is known as the ***scrape-off layer (SOL)*** or the edge plasma region. Our study is focused on this region.

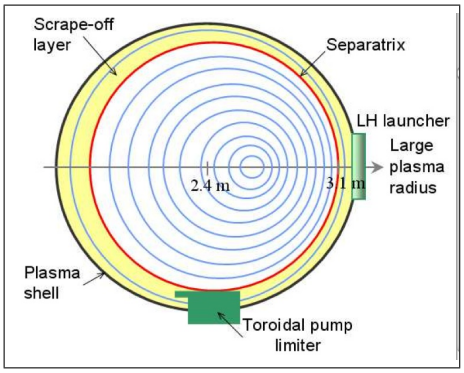

Figure 1.11: Representation of TS section. Source: [6]

Chapter 2

Problem formulation and project objectives

In this chapter, the problem to be solved and the project objectives are stated. For that, the *LH coupling efficiency* problematic, and with it, the *source term* in the SOL will be introduced. Then, the basis of the proposed *blind identification method* is explained. Finally, the project objectives and schedule are stated.

2.1 LH current drive efficiency and The source term

As it was explained in the previous chapter, the Lower hybrid antenna has the objective to launch the electromagnetic waves at the lower hybrid frequency to the center of the plasma with the aim of achieving the toroidal current in it.

But it has been shown that the plasma in the SOL is not "transparent" to the LH waves (as it would be desired to be), and thus, the LH wave-plasma coupling is influenced by the particle density in the SOL as it is stated in [8]. That's why a good knowledge of the LH power - SOL particle density relation would be important to improve the coupling between confined plasma and the waves emitted by this antenna.

When the LH antenna is activated, an increase in the particle density in the SOL can be observed. Nowadays there are two different approaches that explain this density increase.

1. Since the LH antenna increases the plasma temperature, the energy contained in the plasma also increases. In the other hand, when the plasma energy increases the confinement quality decreases (i.e. the transversal diffusion coefficient rises) and thus, this fact could explain the density increase that is experienced in the SOL when the LH heating is applied. (See [9]).

2. The second approach used to explain this density modification due to the LH power states that, due to the temperature increase, the deuterium gas contained in the tokamak walls leaks to the scrape off layer (process known as outgassing) and is ionized by the LH waves (as we have already said, the plasma in the SOL is not transparent to the LH waves and thus, a small fraction of this antenna will be used in ionize this gas), acting as a particle source. This particle source is known as the ***source term***, and it can be defined as the number of electrons par volume and time units that are unintentionally introduced in the scrape-off layer because of the ionization

processes due to the plasma interaction with the limiter (LPT) and the LH-antenna power (local effect).

As a first assumption, we will follow this second approach by trying to identify the source term in the SOL. As it has been said before, the density in the SOL (and thus the source term) is related to the LH coupling efficiency, so a good knowledge of this term could be a key parameter to improve the LH efficiency. To identify this source term we will use the particle density measurements obtained from ***reflectrometry*** diagnosis.

Since the density distribution in the fusion plasma is almost symmetrical with respect to the angular variables, we will study the distribution in the radial direction of a given tokamak section (i.e, the particle density will be distributed along the radial direction).

2.2 Blind identification of system inputs

Up to this section, the project's physical background (thermonuclear controlled fusion in tokamaks) has been elaborated. Now, the project's second main aspect, the identification topic, will be exposed.

Identification techniques are those procedures used in control theory that make possible to "identify" the different coefficients appearing in the equation modeling the system under study. This identification methods normally use the measured output variables of the system when a known (measured) input variable has been applied. Since the input and the output of the system are known variables, there are different mathematical procedures that allow us to find the appropriate model parameters.

But our problem under study is slightly different given the fact that the term that we aim to identify is the input variable itself (the so-called source term). To distinguish this particular problems from the first ones, they are known as ***blind identification problems***. This designation alludes to the fact that we don't have information about the input that is being introduced in the system (as it happens in our problem). Besides, the model parameters are also quite uncertain. The schematics of the general identification problem can be seen in figure 2.1.

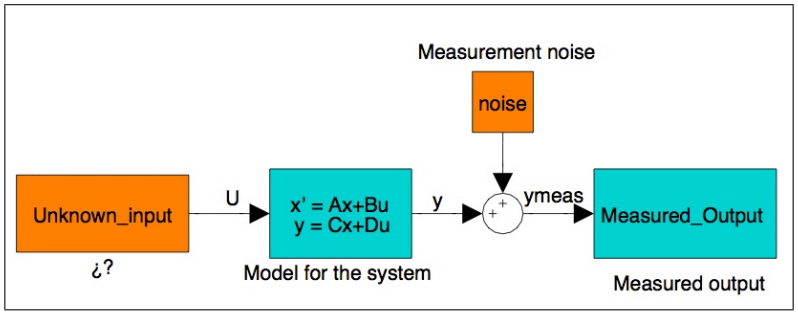

Figure 2.1: Schematic representation of the generalized blind identification problem

In this project, the innovating approach proposed in [7] is applied to solve the blind identification problem. Using the information given by the output density measurements, we find the optimal input that should be introduced in the system to have the minimum tracking error. That is to say, an optimal tracking controller will be used to find the optimal input (the optimal source term in this

case) to obtain the given output (the measured particle density). In figure 2.2 the schematics of this procedure is presented.

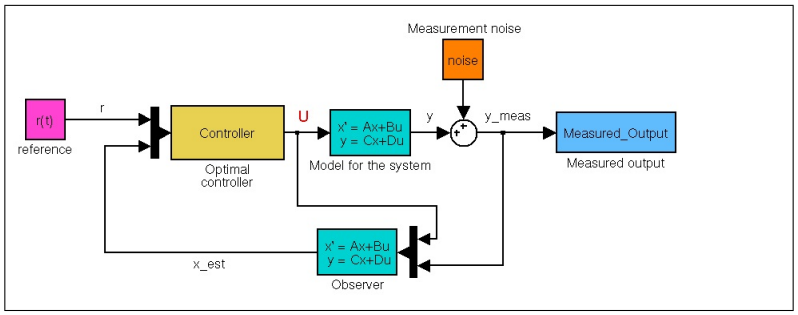

Figure 2.2: Schematic representation of the "optimal" blind identification problem

In appendix F section A, the general optimal tracking solution is expounded..

2.3 Project statement and objectives

Now that the necessary concepts to understand the project background and the problem has been introduced, the project objectives can be exposed.

"In this project, our goal is to identify the particle ***source term*** *appearing in the Tore Supra tokamak's* ***scrape-off layer*** *using* ***control identification techniques*** *and study its possible relation with the power emitted by the* ***Lower Hybrid antenna****.*

Once the optimal source term will have been properly identified, we will establish the basis for an ***online estimation*** *structure to calculate the SOL model time-variant parameters that may be developed and used in subsequent projects."*

To achieve this two final objectives, the following intermediate goals were fixed during the project development (objectives 1-4 were studied within the GIPSA-lab, while objectives 5-7 where studied in the IRFM-CEA):

1. Documentation and analysis of the identification problem.
2. Design, coding, verification and tuning of a first identification structure supposing a simple SOL model.
3. Constraints imposition for the term source.
4. Design of the online parameter estimation structure for the time-varying parameters of the SOL model in a theoretical scenario.
5. Documentation in thermonuclear controlled fusion in tokamaks and SOL plasma physics.
6. Second identification structure using advanced SOL model and parameters.
7. Correlation study of the different terms in the SOL transport model to tune the model parameters.

2.4 Project scheduling and tools

An approximate schedule of the project and its objectives is done next.

Work developed in the *GIPSA-lab* from February to April:

- [1/02 – 14/02] : Initial documentation in optimal control and EDP systems.
- [15/02 – 28/02] : First tracking structure. Verification scenario.
- [1/03 – 10/03] : Cost function tuning and time-varying boundary conditions.
- [11/03 – 21/03] : Verification of the algebraic approach hypothesis.
- [22/03 – 9/04] : Third tracking structure: Introduction of the constraints. Linearization. Equilibrium source.
- [10/04 – 15/04] : Numerical problems identification and dealing.
- [16/04 – 30/04] : Online parameters estimation: Documentation and first estimation structure. Verification.

Work developed in the *CEA-IRFM* in May and June:

- [03/05 – 16/05] : Initial documentation in plasma physics and thermonuclear fusion.
- [17/05 – 21/05] : 2 zones model (without sink term for the confined plasma and with sink term for the SOL)
- [21/05 – 30/05] : 3 zones model (2 diffusive + convective in the SOL)
- [31/05 – 8/06] : Model parameters documentation and computation.
- [5/06 – ...] : Model parameters tuning (correlation)

I worked full-time in both institutions, the GIPSA-lab (from 9h to 17h) and the CEA-IRFM (8h to 16h). Apart from developing this project, in both institutions i assisted to seminars and conferences that enriched this internship experience.

Matlab® and its simulation tool, *Simulink*®, are the main technical software that have been used during this project.

In the following chapters the main results obtained during this project internship will be presented.

Chapter 3

Optimal source identification structure

In this chapter, the development and the results concerning to the optimal identification structure achieved during this first part of the project are detailed. At first, the identification structure itself is presented, next, the verification and tuning processes are briefly exposed, then the identified source term obtained using real Tore Supra data measurements is shown and finally, the improved structure due to the insertion of dynamical boundary conditions and the improved source term are exposed.

3.1 First model and identification structure

The first transport model used for the SOL was a completely diffusive transport model deduced from [6]:

$$\frac{\delta n(x,t)}{\delta t} = D_{\perp}\frac{\delta^2 n(x,t)}{\delta r^2} - \gamma n(x,t) + S(x,t) \tag{3.1}$$

where n stands for the particle density (i.e. electronic density), $D_{\perp}$ is the transversal diffusion coefficient, γ is known as the sink term and represents the particle losses in the SOL, and $S(x,t)$ is the source term that represents the supposed particle introduction due to ionization and transport phenomena in the SOL and in the limiter (see appendix D for further information about the models). For this first part of the project, approximate values were chosen for the parameters $D_{\perp}$ and γ.

The following distributed state space representation was obtained once the previous model had been space-discretized in N points (both, the discretization and the state space obtention are detailed in appendix E):

$$\dot{\mathbf{n}} = A \cdot \mathbf{n}(\mathbf{t}) + B \cdot \mathbf{S}(\mathbf{t}) + \omega \tag{3.2}$$

where $\mathbf{n} = [n_1, n_2, ..., n_N]$ is the distributed density vector, S(t) is the input source term to be identified and ω is a known disturbance vector containing the boundary conditions for the problem.

To identify the source term, as it was explained in section 2.2, an optimal LQR tracking controller will be applied. Since it will be used for identification purposes, an integral action will be added to the system in order to avoid steady state error (the resulting extended state system is shown in appendix E section C). The controller was computed under certain hypotheses (see Algebraic approach section in appendix F section B) that were verified later on. The resulting *optimal identification structure* is

shown in figure 3.1. Constant boundary conditions based in mean measurements were chosen in this first stage.

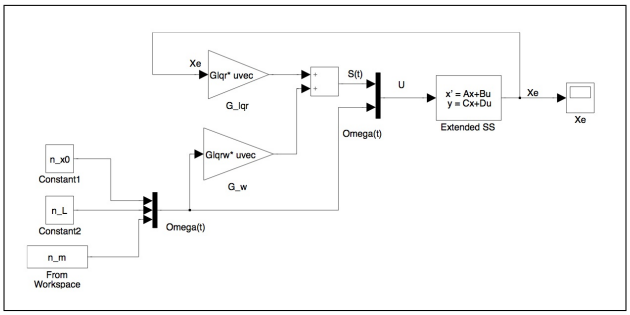

Figure 3.1: Optimal identification structure

3.2 Structure verification. Q and R tunning

To test the performance of the structure, a verification test was carried out. Inserting an hypothetical gaussian particle source, $\mathbf{S}(t)$, in the model (3.1), a theoretical density distribution, $\mathbf{n}(t)$, was obtained. This distribution was introduced in the identification structure and the gaussian source was retrieved. This test can be seen in figure 3.2.

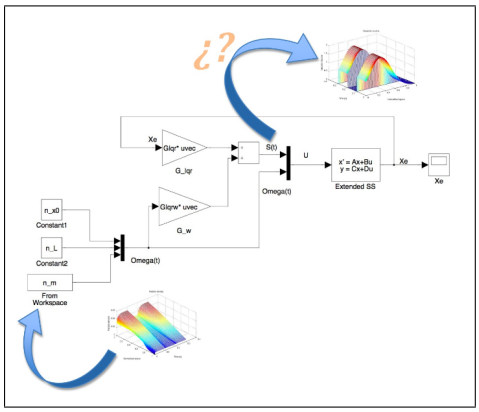

Figure 3.2: Verification scheme

Figure 3.3 shows the identified source term and the normalized tracking error (defined as $e(x,t) = \left|\frac{n_{measured}(x,t) - n_{model}(x,t)}{n_{model}(x,t)}\right|$) when the weighting matrices for the LQR are chosen as $Q = R = I$

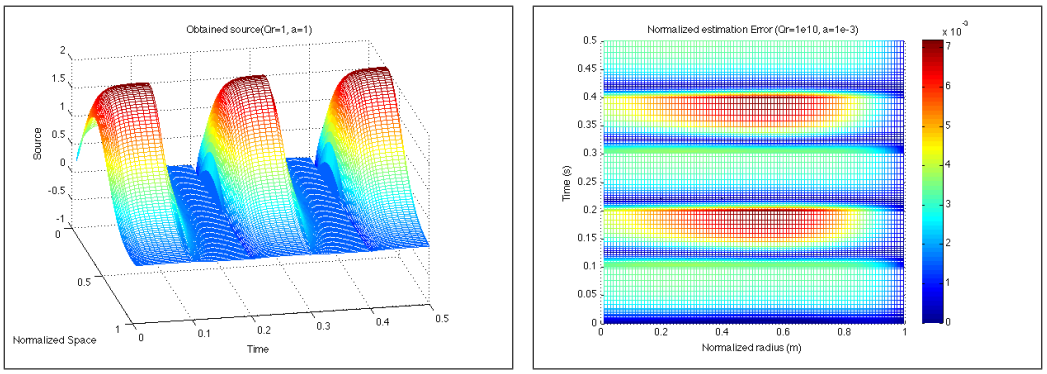

(a) Obtained theoretical source term

(b) Normalized tracking error

Figure 3.3: Obtained source term and tracking error for $Q = Id$ and $R = Id$

After studying these results, it was noticed that the estimation error, although small, was always persistent (fig. 3.3b). Since an integral action had been added to the system, the steady state error should be nil, so we deduced that the problem was that the settling time, so the weighting matrices should be readjusted to speed it up. In fact, after studying the problem, it was stated that the bigger the Q/R ratio, the faster the error was compensated. In the following graph it can be seen the improvement in the obtained source and tracking error when the weighting matrices were chosen as $Q = Id \cdot 10^7$ and $R = Id \cdot 10^{-7}$

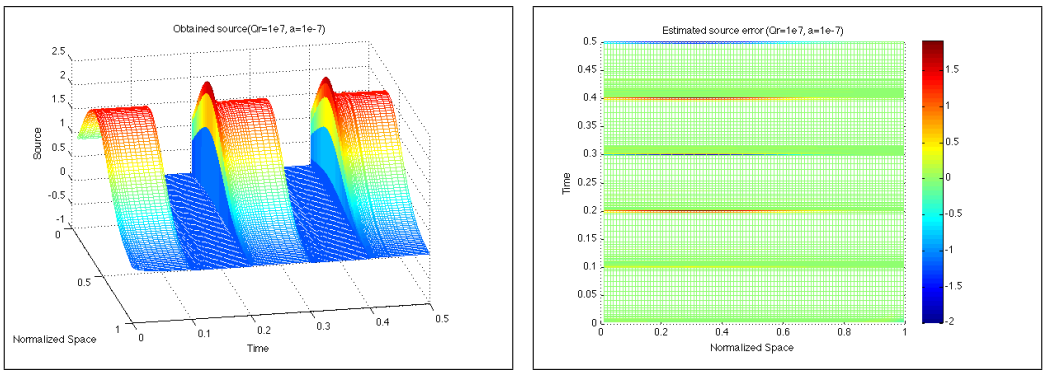

(a) Obtained theoretical source term (b) Normalized tracking error

Figure 3.4: Obtained source term and tracking error for $Q = I \cdot 10^7$ and $R = I \cdot 10^{-7}$

3.3 Application to real data shot TS38953

Once the identification structure had been checked and tuned, the Tore Supra density measurements from shot TS38953 were applied. In this shot, the LH antenna was being constantly switched on and off (see appendix H for further information about the data shots used during this project). In figure 3.5 the measured density and the accumulated tracking error performed ($\bar{\mathbf{e}}(t) = \frac{1}{x_f - x_0} \sum_{i=0}^{N} (\mathbf{e}(x_i, t)\Delta x_i)$) by the identification structure are shown. The identified source term can be observed in figure 3.6.

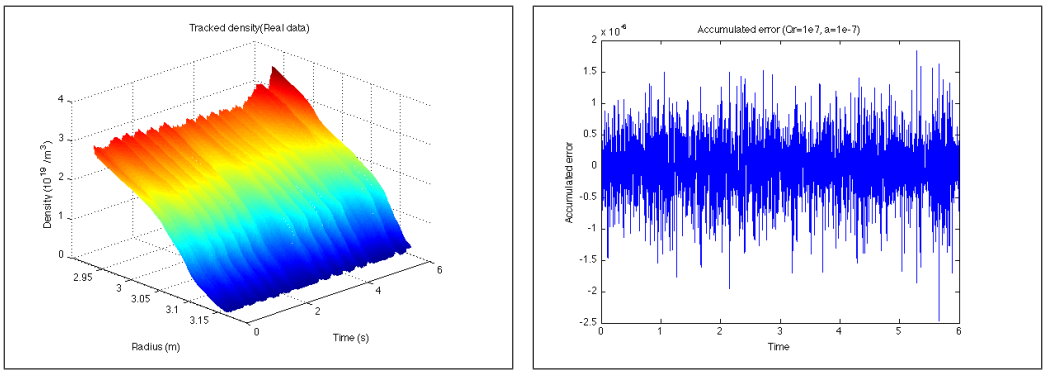

(a) Tracked density (b) Accumulated tracking error

Figure 3.5: Tracked density and accumulated tracking error from TS38953

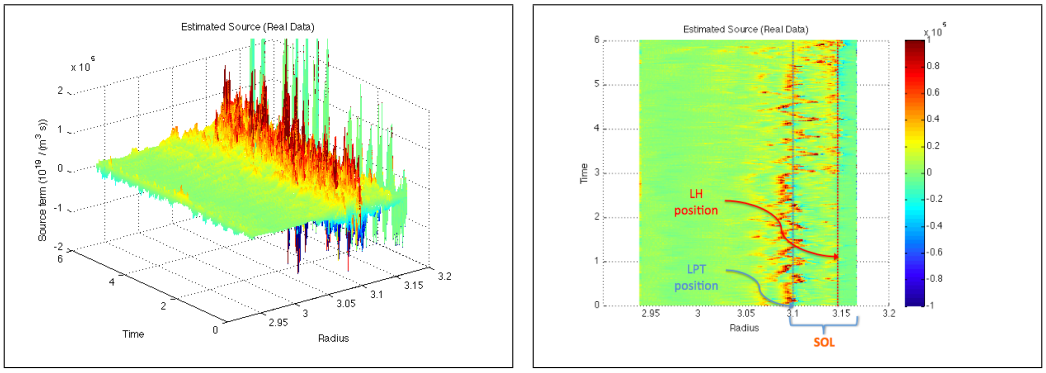

(a) Identified source term for TS38953 (b) Top view of the identified source

Figure 3.6: Identified source term for TS38953. LH modulation detail

As it was supposed, two sources appear in the SOL, one due to the limiter (LPT) and the other one due to the LH antenna. So, the source term can be written as:

$$S(x) = S_{LPT}(x) + S_{LH}(x)$$

where $S_{LPT}(x)$ is larger than $S_{LH}(x)$. Also, a plasma displacement when the LH power is on can be observed.

But in this identified source two main problems appear. The first one is that the source term reaches negative values, which cannot happen in the real source term. Also, the positive values reached by the source are much higher than it was expected (order 10^2). The second problem is that edge distortion appears in the source due to the constant boundary conditions that had been chosen. This problem will be solved in the following section.

3.4 Structure improvement: Time varying boundary conditions

To solve the edge source distortion problem, time varying boundary conditions were added to the extended state of the system. The procedure that was used to include the boundary conditions in the system can be read in appendix E section F. In figure 3.7 the new identification structure is shown.

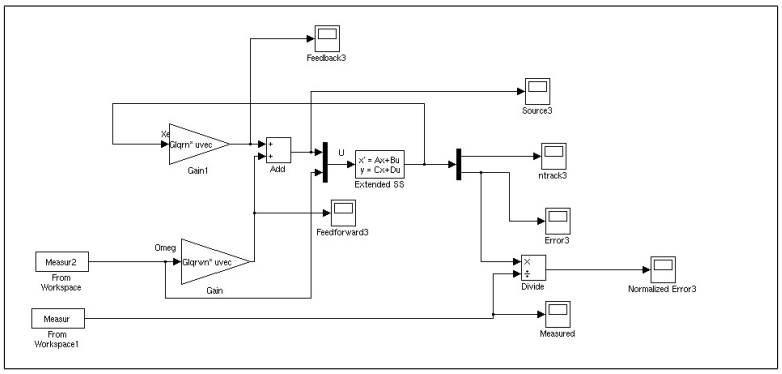

Figure 3.7: Second identification structure

As it can be seen, boundary conditions are no longer introduced as a external parameter. The structure uses the measurement information to generate the appropriate conditions for every instant instead of using constant boundary condition based on mean measurements.

In the following figure we can observe the source term identified with the new structure. As we can see, the edges are no longer distorted. In the other hand, the rest of the term doesn't suffer substantial changes and the order of magnitude for the density accumulated tracking error is maintained as 10^{-6}.

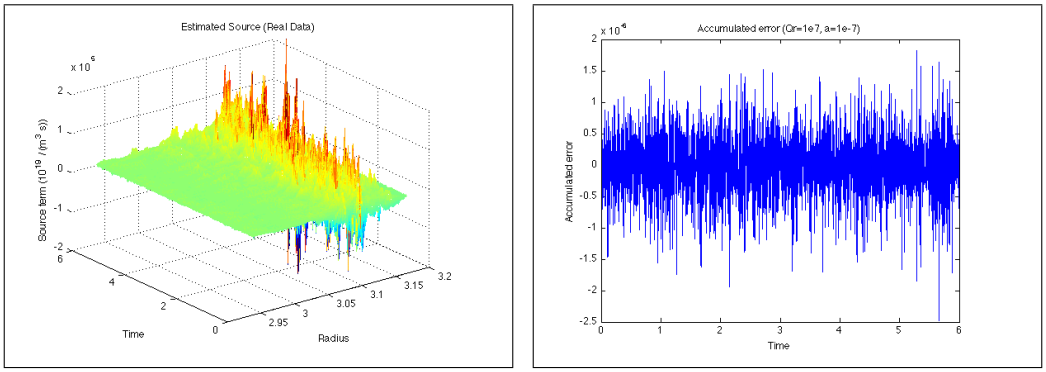

(a) Identified source term with varying conditions (b) Accumulated density tracking error

Figure 3.8: Obtained results for the TS38953 shot using the new structure

3.5 Application to real data shot TS45525

Due to the high values obtained with data shot TS38953, we decided to try the structure with another data shot obtained from Tore Supra, the shot TS45535. This shot, unlike the first one, was obtained using constant LH heating power (see appendix H for further info about data shots). The density distribution for the new shot and the results obtained can be seen in the following figures.

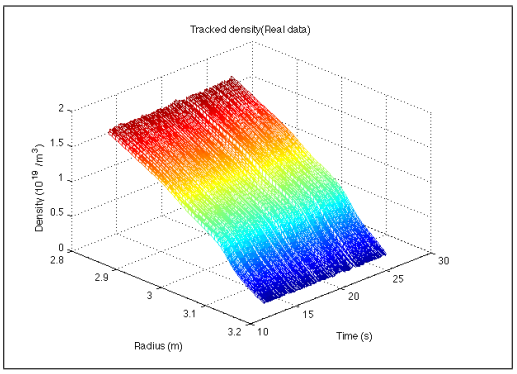

Figure 3.9: TS45525 density distribution

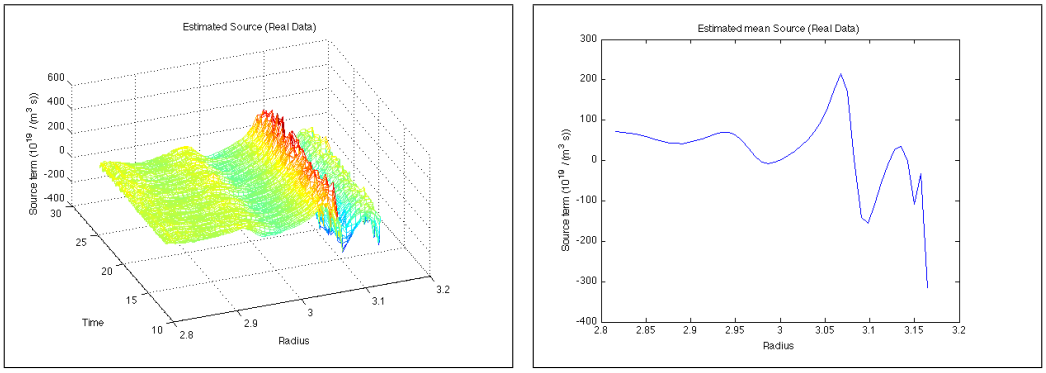

(a) Identified source term with varying conditions (b) Mean source term values

Figure 3.10: Obtained sources for the TS45525 shot

It can be observed that, even if negative values keep appearing in the source term, now the order of magnitude of the sources is around the expected one. So we can say that further studies will be needed to identify the cause of the high source term obtained when the LH power changes abruptly.

In the new source term, it can be observed a third peak (in the middle of the LPT source and LH source). This third source can be caused by the antenna protection limiter (LPA) that was not taken off during the TS45525 shot (unlike in TS38953, where it was removed especially for that experience). In fact, the position of the plasma facing components during this shot were:

- LPT: $R = 3.086$ m
- LPA: $R = 3.116$ m
- LH: $R = 3.153$ m

That correspond approximately with the source peaks position. So we can conclude that the new obtained source is more coherent with the expected values. In the other hand, we can see that the source term in the confined plasma always present positive values (though small), and we know the source term in confined plasma must be nil. This problem will be solved in other section.

Chapter 4

Constrained optimal identification

With the aim of trying to avoid negative values in the source term, a constrained identification structure was designed so that a determined shape could be imposed to the input source term. In this chapter, the deduced constrained system and the constrained equilibrium source are first introduced. Then, the designed constrained identification structure and the numerical issues observed during its application to the real system are exposed.

4.1 Constrained system. Equilibrium gaussian source term

From [6], the assumption of a SOL source term composed by two gaussian distributions (one due to the LPT and the other one due to the LH antenna) was taken. The main idea consists in changing the arbitrary distributed input source used up to this moment for a gaussian shaped distributed source parametrized by the amplitude, θ, the mean, μ, and the standard deviation, σ, of the two gaussian distributions:

$$S(x,t) = \theta_{LPT}(t)e^{-(x-\mu_{LPT}(t))^2/(2\sigma_{LPT}(t)^2)} + \theta_{LH}(t)e^{-(x-\mu_{LH}(t))^2/(2\sigma_{LH}(t)^2)}$$

Then, the constrained discretized system would be:

$$\begin{cases} \tilde{n}_{t,1}(t) = \frac{\alpha}{\Delta x^2}\tilde{n}_2(t) - (\frac{\alpha}{\Delta x^2} + \gamma)\tilde{n}_1(t) - \frac{\alpha}{\Delta x}\tilde{n}_{x0}(t) + \overbrace{\sum_{j=l,LH} \theta_j(t)e^{-(x_1-\mu_j(t))^2/(2\sigma_j(t)^2)}}^{S_1(t)} \\ \vdots \\ \tilde{n}_{t,i}(t) = \frac{\alpha}{\Delta x^2}\tilde{n}_{i+1}(t) - (\frac{2\alpha}{\Delta x^2} + \gamma)\tilde{n}_i(t) + \frac{\alpha}{\Delta x^2}\tilde{n}_{i-1}(t) + \overbrace{\sum_{j=l,LH} \theta_j(t)e^{-(x_i-\mu_j(t))^2/(2\sigma_j(t)^2)}}^{S_i(t)} \\ \vdots \\ \tilde{n}_{t,N} = \frac{\alpha}{\Delta x^2}\tilde{n}_L(t) - (\frac{2\alpha}{\Delta x^2} + \gamma)\tilde{n}_N(t) + \frac{\alpha}{\Delta x^2}\tilde{n}_{N-1}(t) + \overbrace{\sum_{j=l,LH} \theta_j(t)e^{-(x_N-\mu_j(t))^2/(2\sigma_j(t)^2)}}^{S_N(t)} \end{cases} \quad (4.1)$$

So now, the input to the system is not the source term but its gaussian parameters

$$\vartheta(t) = [\theta_{LPT}\ \mu_{LPT}\ \sigma_{LPT}\ \theta_{LH}\ \mu_{LH}\ \sigma_{LH}]'$$

Since the constrained system was non linear with respect to the input variable, ϑ, it had to be linearized around an equilibrium point; this equilibrium point is what we call the equilibrium source. The obtained linearized system can be seen in appendix E section E.

The parameters ϑ for the gaussian equilibrium source were computed such that the error between the obtained density and the mean measured density was minimized. This process can be seen in appendix E section E. The following plot shows the obtained equilibrium source and the equilibrium density.

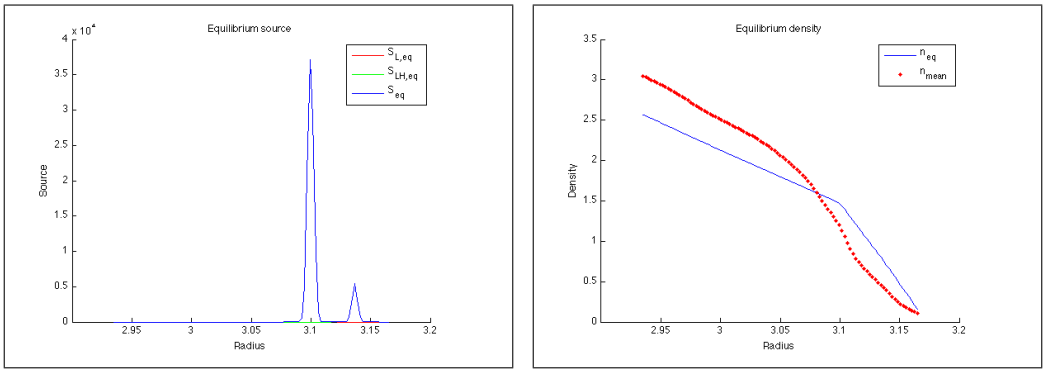

(a) Equilibrium gaussian source

(b) Corresponding equilibrium density and mean density

Figure 4.1: Optimal equilibrium gaussian source and density

This source represents the optimal constrained (gaussian like) input for the system in order to obtain the equilibrium density, taken as the mean density.

4.2 Constrained identification structure. Numerical difficulties

Once the system was linearized around the equilibrium source, a constrained identification structure was designed to obtain the gaussian-like source term varying in time. This identification structure can be seen in figure 4.2.

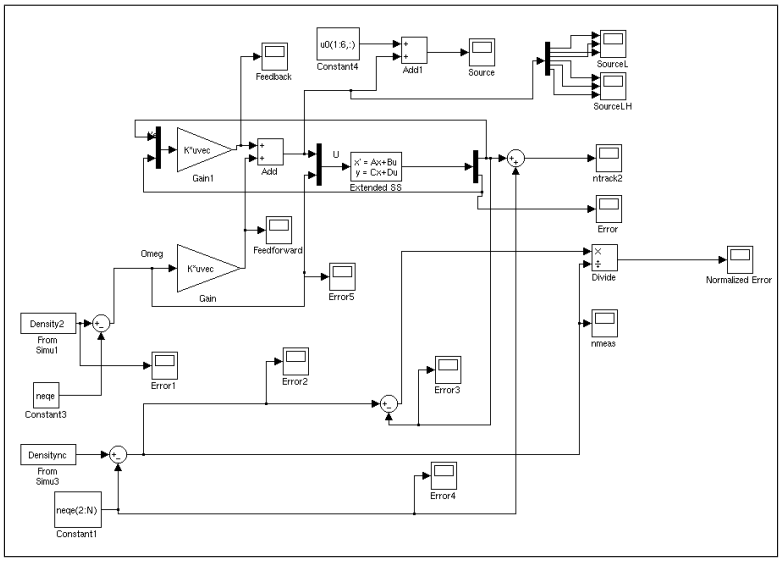

Figure 4.2: Constrained identification structure

This structure would retrieve the incremental gaussian parameters (the input to the linearized constrained system) and calculate the corresponding gaussian shaped source (SourceLH and SourceL in the scheme).

Unfortunately, although the performance of this identification structure was verified with more simple systems, when the system under study (the constrained linearized input system) was implemented, numerical problems took place and the solution for the LQR optimal controller could not be found. After studying this situation, we arrived to the conclusion that the difficulty lied in solving the Ricatti equation F.18. To solve this sort of equations, the *Matlab*® function *care* (the one used to obtain the optimal controller in the unconstrained structure), computes the eigenvalues of the Hamiltonian matrix:

$$\mathcal{H} = \begin{pmatrix} A_e & -B_{e1}R^{-1}B'_{e1} \\ -Q & -A'_{en} \end{pmatrix}$$

For the constrained case, *Matlab*® justifies that the eigenvalues of this matrix are too near to the imaginary axis, and thus, it cannot find the solution to the Ricatti equation. In figure 4.3 this matrix eigenvalues can be observed.

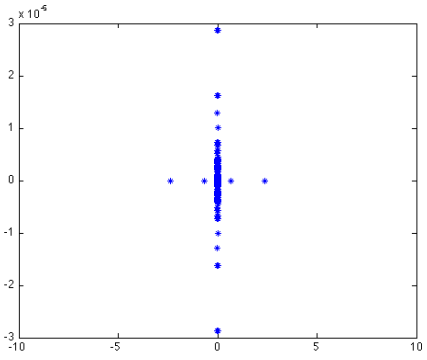

Figure 4.3: Hamiltonian matrix eigenvalues

We have not been able to solve this problem up to this moment, so, further research will be needed. Nevertheless, the previously obtained equilibrium source can be used in other stages of the project (the time varying model coefficients estimation structure).

Chapter 5

Model revision and improvement

The previous stages of the project have been focused in achieving the most accurate SOL identification structure in order to retrieve a source term with an expected shape. Now, we will focus in improving the SOL model that has been used up to this moment. In this chapter, a new SOL model based in 3 different regions is deduced. Then, an accurate calculation of the transport parameters is done, and finally, the last stage of the project is dedicated to the design, in a theoretical scenario, of an online estimation structure to estimate the optimal value of the time varying model parameters and thus, improve the SOL model.

5.1 Compartmental description with a 3-zones model

Working in the IRFM, we arrived to the conclusion that a more complex and accurate transport model for the SOL was needed. From [12] we took the assumption that a convective model may be more appropriated for the last part of the SOL (until this moment we had been using a simple diffusive one). In addition, for the plasma placed before the separatrix (i.e. confined plasma), there would be no sink term since the magnetic field lines in confined plasma are closed on themselves. So now, the edge plasma region in which we were working was split in three different subregions: Confined plasma, first part of SOL and final part of SOL. We had, thus, the following transport models:

- Diffusive model (used in the confined plasma region)

$$\frac{\delta n(x,t)}{\delta t} = D_{\perp}\frac{\delta^2 n(x,t)}{\delta r^2} + S(x,t) \tag{5.1}$$

- Diffusive model with sink term (used in the first part of non confined plasma region or scrape off layer)

$$\frac{\delta n(x,t)}{\delta t} = D_{\perp}\frac{\delta^2 n(x,t)}{\delta r^2} - \gamma n(x,t) + S(x,t) \tag{5.2}$$

- Convective model with sink term (used in the second part of non confined plasma region or scrape off layer)

$$\frac{\delta n(x,t)}{\delta t} + V_c\frac{\delta n(x,t)}{\delta r} = -\gamma n(x,t) + S(x,t) \tag{5.3}$$

For further information about these transport models, their parameters and their application regions in the plasma section see appendix D.

To integrate these three models in the same state space representation, they had to be connected through boundary conditions in each region transition. The resulting 3-model state space can be seen in appendix E section F.

5.2 Parameters computation and obtained source term

Once the new state space representation was obtained, the different model parameters had to be conveniently chosen. After studying the problem, the parameters were finally calculated as stated in appendix D. The code for this fourth identification structure was conceived to allow space-varying parameters for the models, which is a more realistic situation than the previous one (It must be noticed that, up to this moment, the model parameters had been supposed as constants).

In figure 5.1 we can see the obtained source term for the data shot TS45525 (see appendix H for further information about data shots) using the 3-region model and the parameters shown in figure 5.2. We must remember that the TS45525 shot was obtained from a tokamak experience where the power input from the LH antenna was set as constant.

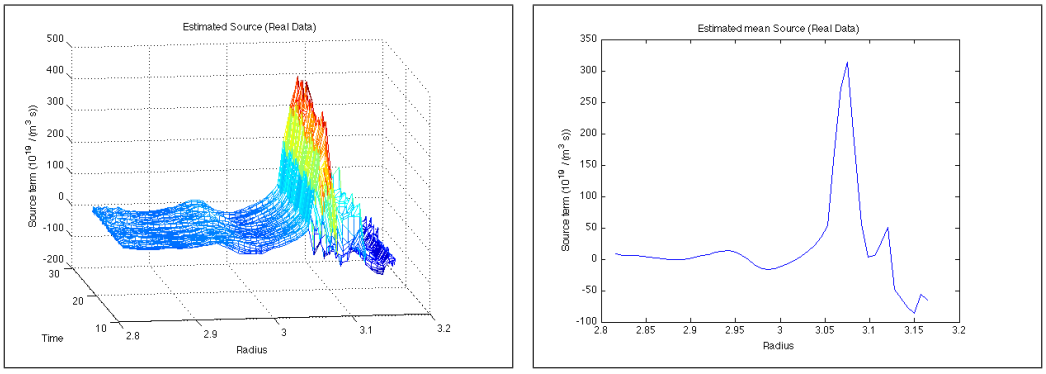

(a) Identified source term with 3-zones model (b) Mean source term values

Figure 5.1: Obtained sources for the TS45525 shot using the 3-zones model

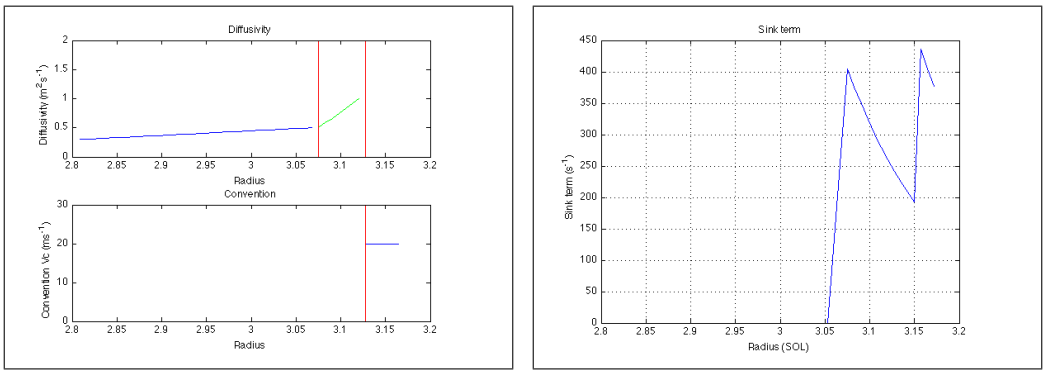

(a) Values for the $D \perp$ and the Vc coefficients (b) Values for the sink term

Figure 5.2: Calculated parameters for the 3 zones model

Comparing these results with the ones obtained with the first estimation structure (fig. 3.10) it can be observed that the negative values have been reduced and the values for the three sources that keep appearing are more coherent with the expected values. Also, it can be seen that the source term in confined plasma is practically. So we can say that the new model seems to be more accurate.

But, it is important to notice that the obtained source term is very sensible to variations in the model parameters. That's why we consider that finding the optimal value for this parameters is critical. The following section is the first step to achieve this goal.

5.3 Online parameter estimation structure. Theoretical scenario

It must be noticed that the transport coefficients or parameters have a very strong impact in the resulting source term. It must be also noticed that these parameters are very uncertain even if they have been properly calculated. The aim of this last stage of the project is to establish the basis for an online parameter estimation structure to obtain the time-varying model parameters $D_\perp(t)$, $\gamma(t)$, $Vc(t)$, and $s(t)$ (parameter multiplying the source term) that minimizes the error between the measured density and the tracked density using the previously obtained sources. Thus, with this estimation structure we want to achieve a fine tuning for both, the previously obtained sources (modulated by the new parameter s(t)) and the SOL model (by retrieving the optimal $D_\perp(t)$, $\gamma(t)$ and $Vc(t)$ values).

In this project, this structure has been developed under a theoretical scenario and using the first SOL model (simple diffusive model) in order to test it performance. Further work will be focused in developing and applying this initial structure to be used under the 3-model system scenario and using real TS data shots.

The estimation structure has been developed using the estimation theorem deduced in [14]. This theorem and the development process of the estimation structure can be read in appendix G. The scheme of the resulting structure can be seen in the following figure (fig. 5.3).

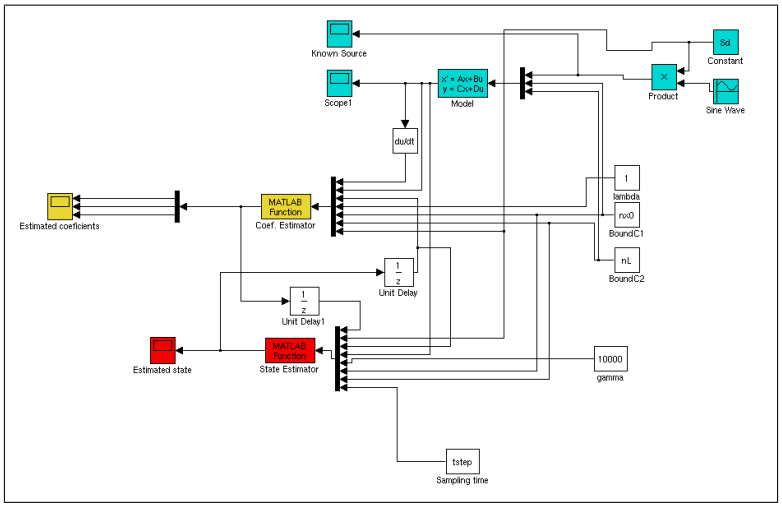

Figure 5.3: Online estimation structure

To verify the designed structure, the procedure that was followed was to create a theoretical density distribution using a Gaussian source that had been modulated with a sinus function. As we

can see in the following simulation results, the structure succeeded to retrieve the model parameters and the source term modulation with a small error (fig. 5.5).

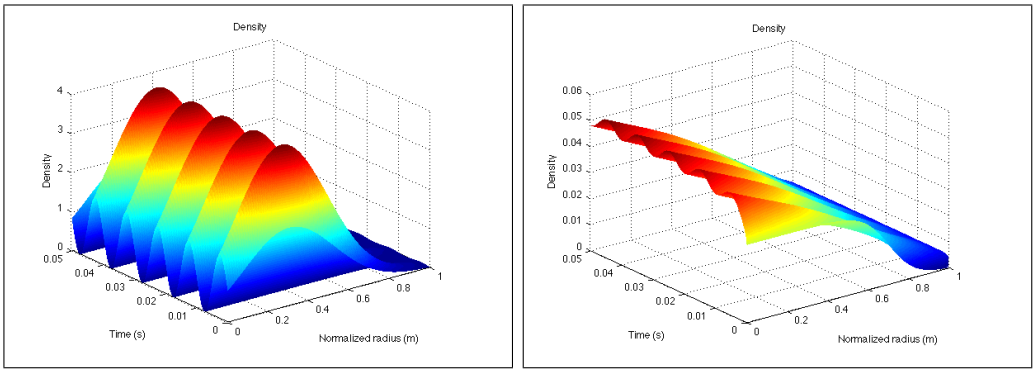

(a) Introduced source to obtain the density (b) Obtained theoretical density

Figure 5.4: Theoretical source and density to be used in the verification scheme

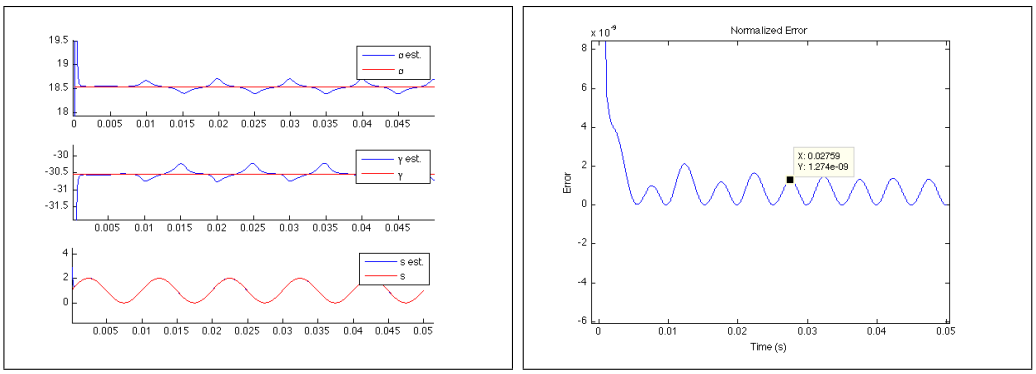

(a) Estimated and real parameters (b) Normalized estimation error

Figure 5.5: Parameters estimation results

This fact proves the estimation structure utility in this kind of problems, and thus, we can conclude that future work is worth to develop the estimation structure and apply it to this (and other) problem with the aim to improve the SOL model.

Chapter 6

Conclusions and future work

Conclusions

- In this project, we have developed an identification structure allowing us to retrieve the optimal time varying input for a system model when the output is measured.
- Though in this project this structure has been developed for the SOL model in tokamaks, it can be easily extrapolated to other systems.
- This identification method makes possible the use of constraints for the input or multiple region for the models, as we have seen in this project.
- Due to numerical difficulties that stem from the model complexity, the gaussian constraint could not be applied in the real SOL system during this project. Further work will be needed to overcame this issue. Also, smoother constraints could be applied.
- The obtained source term shows effectively the shape of the expected source, but, in the other hand, the value of this source term is strongly related to the model parameters, characterized by a high uncertainty. That's why it is important to find the appropriate value for the parameters in the model in order to obtain an accurate source term.
- The first results for the developed parameter estimation structure in the theoretical scenario show that this can be a powerful tool to calculate the optimal time variant parameters for the model. Though further work will be required in order to overcome the difficulties and adapt this model for the real scenario, the expectation seems to be good.

Future work

Future investigation lines may be centered in:

- Solving the numeric problems in the constrained source identification structure.
- Developing and applying the online parametric estimation structure in the real scenario.
- Studying the optimal estimated parameters to improve the SOL model and the source term.
- Applying the identification structure to study plasma fast dynamics (TS38953).
- Design a combined structure including both, the identification and estimation structures.

APPENDICES

Appendix A

Internship workplace: GIPSA-lab and IRFM-CEA

This project has been carried out within two laboratories in collaboration: the GIPSA-lab and the IRFM. The 3 months research in the GIPSA-lab was mainly dedicated to the study and design of the identification methods that would be applied later on in the experimental fusion tokamak reactor, Tore Supra, operated by the IRFM. In this second institution, the gained knowledge in plasma physics and magnetic confinement thermonuclear fusion made possible the improvement and adaptation of the previously designed identification methods to be applied in tokamak fusion plasmas.

A GIPSA-lab

The GIPSA-lab (Grenoble Images Parole Signal Automatique) is a research institution that belongs to the French CNRS (Centre National de la Recherche Scientifique), the INPG (Institut National Polytechnique de Grenoble), the UJF (University Joseph Fourier) and the Stendhal university. It's located within the INPG site (Grenoble, France)

The institution research activity is mainly centered in the development of advanced control methods, signal and image processing procedures and system diagnosis. Due to the large range of possibilities in which these methods can be applied, the GIPSA-lab keeps contact with a very large range of different fields that covers from telecommunications to energy systems (as in this project). To carry on this research work, the GIPSA-lab bases in the latest theories in control and signal processing.

Figure A.1: GIPSA-lab

The staff in the GIPSA-lab is composed by around 300 people where 70 are university professors, 30 are CNRS researchers, 40 technicians, 120 phD students and around 80 master students and guest researchers. All of them are organized in 3 main departments:

- Control.

- Image and signal processing.
- Language and knowledge.

My 3 months work in the GIPSA-lab was realized for the Control department under the guidance of Mr. Emmanuel Witrant.

B Euratom-CEA: IRFM

The CEA-IRFM (Institut de Recherche sur la Fusion par confinement Magnétique) is the French associated member for the Euratom program (unified fusion research program in Europe) an thus, the institution in charge of the thermonuclear controlled fusion research in France. This institute is part of the CEA organization (Commissariat à l'Énergie Atomique), and it's located in the CEA site at Cadarache (Bouches-du-Rhône, France).

Figure A.2: CEA-IRFM

The IRFM exploits the Tore Supra tokamak, working since 1988. This is the first world large tokamak built with superconducting magnets. It is in this tokamak that this project takes place.

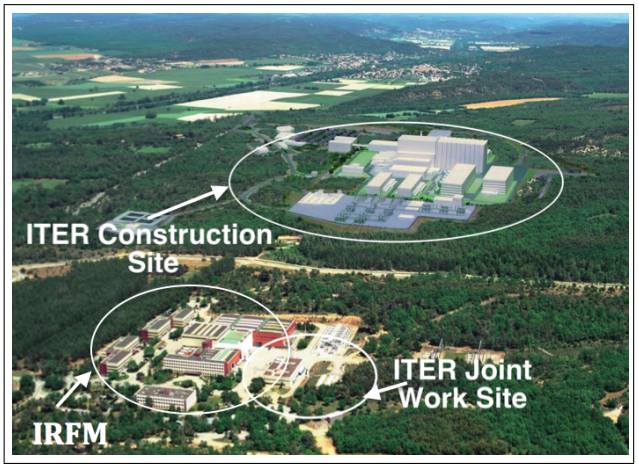

Figure A.3: IRFM location and future ITER emplacement

The IRFM, as an Euratom association, is involved in the ITER project, the global thermonuclear fusion program that aims to prove the viability of thermonuclear controlled fusion as a reliable power source.

The staff in the IRFM is composed by around 300 researchers and employees and around 25 temporary collaborators and 20 research students. The institute is organized in 3 main departments.

- Heating and plasma confinement (SCCP)
- Plasma-Wall integration (SIPP)
- Tokamak exploitation and control (STEP)

During my 2 months internship at the IRFM, I worked for the SCCP department, specifically for the high frequency heating and current drive team (GCHF), under the guidance of Mr. Marc Goniche.

Appendix B

Units and Energy density comparative

A Conversion factors for units

From	**TJ**	**Gcal**	**Mtoe**	**MBtu**	**GWh**
to	*Multiply by*				
TJ	1	238.8	$2.388 \cdot 10^{-5}$	947.8	0.2778
Gcal	$4.1868 \cdot 10{-}3$	1	10^{-7}	3.968	$1.163 \cdot 10^{-3}$
Mtoe	$4.1868 \cdot 104$	10^{7}	1	$3.968 \cdot 107$	11630
MBtu	$1.0551 \cdot 10{-}3$	0.252	$2.5 \cdot 10^{-8}$	1	$2.931 \cdot 10^{-4}$
GWh	3.6	860	$8.6 \cdot 10^{-5}$	3412	1

Equivalents eV

$$1 \text{ eV} = 1.6022 \cdot 10^{-19} J \quad \equiv 1.783 \cdot 10^{-36} \text{ kg} \quad \equiv 11.605 \text{ k} \quad \equiv 3.291011 \cdot 10^{-16} \text{ s}$$

B Energy density comparative *Source: [3]*

Fuel type	Energy content (MJ/kg)
Pumped stored water at 100 m dam height	0.001
Bagasse (residue from sugarcane)	10
Wood	15
Sugar	17
Methanol	22
Coal	23 - 29
Ethanol	30
LPG (Liquid petroleum gas)	34
Butanol	35
Biodiesel	38
Oil (petroleum average)	42
Gashol (90% gasoline, 10% alcohol)	10
Gasoline	45
Gasoil (Diesel)	48
Methane (gas)	55
Hydrogen (gas)	120
Nuclear fission (U-235)	90,000
Nuclear fusion (H)	300,000
Binding energy of helium (He)	675,000

Appendix C

Tore Supra main features. Main tokamaks comparative **Source: IRFM-TS**

A Tore Supra main components

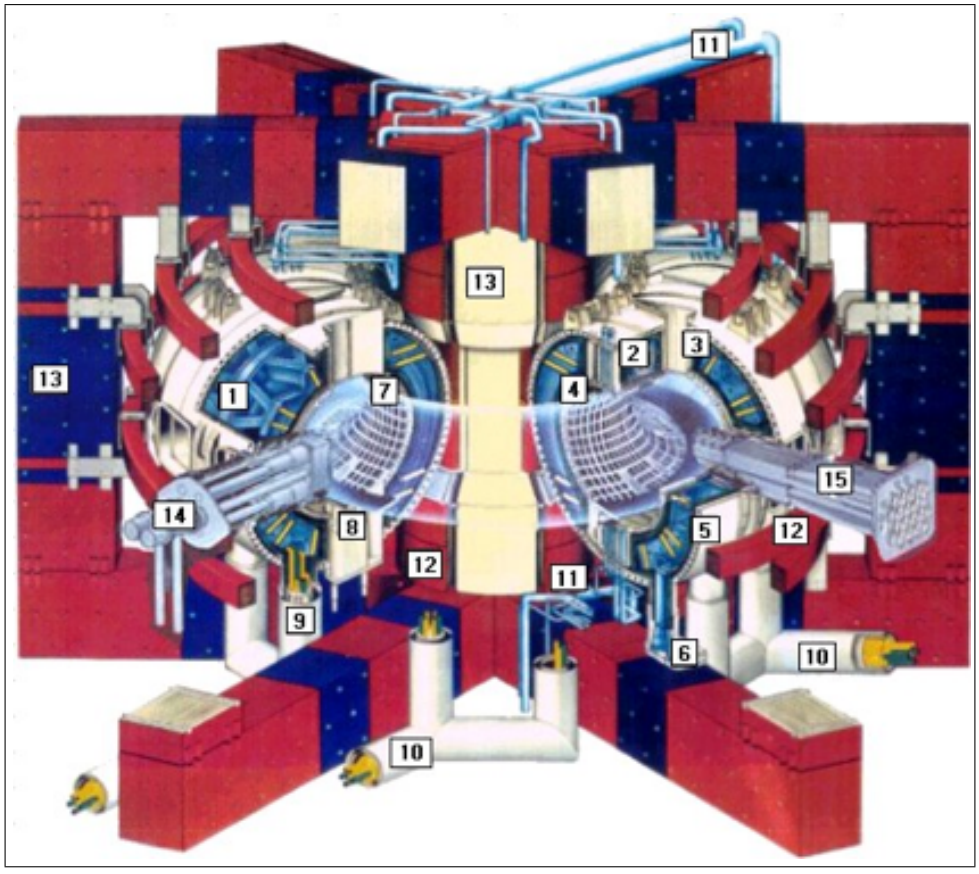

Figure C.1: Schematic representation of the TS tokamak

Reference	Component
1	4 K mechanical structure of coils
2	Superconducting winding
3	80 K thermal screen
4	Cryostat, internal area at $220 \circ C$
5	Cryostat, external area at $20 \circ C$
6	Supporting pedestal for the cryostat and screens
7	First wall actively cooled to $220 \circ C$
8	Toroidal pumped limiter
9	Cryogenic supply, 1.8 K, 4 K and 80 K
10	Towards exchanger, water pressurized at $220 \circ C$, 40 bars
11, 12	Poloidal field coils
13	Magnetic circuit
14	Heating antenna at ion cyclotronic frequency
15	Heating antenna at lower hybrid frequency

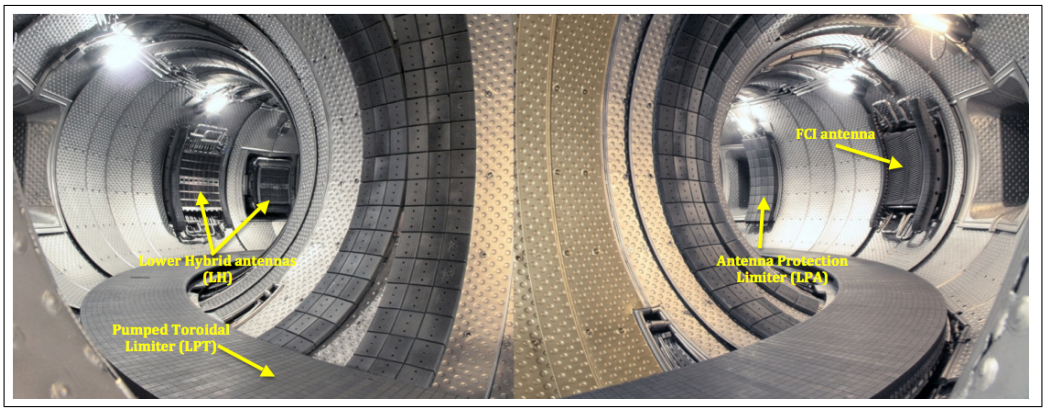

Figure C.2: Tore Supra vacuum chamber and face to plasma components. Modified from TS

B Tore Supra main features

With a major radius of 2.25m (machine centre to plasma centre) and a minor radius of 0,70m, Tore Supra is one of the largest tokamaks in the world. Its main feature is the superconducting toroidal magnets which enable generation of a permanent toroidal magnetic field. Tore Supra is also the only tokamak with plasma facing components actively cooled. Theses two features allow the study of plasma with long pulse duration.

Feature	Value
Major plasma radius	2.40 m
Minor plasma radius	0.68 m
Diameter	11.5 m
Height	7.2 m
Internal vacuum vessel diameter	1.80 m
Total weight of vacuum vessel and heat screens	50 t
Toroidal magnetic field at the plasma center	4.5 T
Maximum magnetic field in the conductor	9 T
Average diameter of a magnet coil	2.60 m
Dimension of the NbTi superconductor	2.8x5.6 mm^2
Weight of superconductor	45 t
Total weight of magnet	160 t
Total magnetic energy	600 MJ
Plasma current	1.7 MA
Potential duration of discharge	1000 s
Weight of central solenoid	56 t
Weight of magnetic circuit	830 t
Cooling power at 80 k	40 kW
Cooling power at 4.5 k	650 W
Cooling power at 1.75 k	300 W

C TS-JET-ITER comparative

Next a comparative of the main features for Tore Supra, JET and ITER (expected) is shown.

Parameter	Tore Supra	JET	ITER
Major plasma radius (m)	2.40	3	6.21
Minor plasma radius (m)	0.68	1.25	2.0
Volume of plasma (m^3)	25	155	837
Plasma Current (MA)	1.7	5 - 7	15
Magnetic field (T)	4.5	3.4	5.3
Duration of pulses (s)	minutes	10	$> 300s$
Type of plasma	D-D	D-D / D-T	D-T
Thermonuclear power (P_{th})	kW	50 kW - 10 MW	500 MW
$Q = P_{th}/P_{heating}$	≈ 0	≈ 1	> 10
Neutron power at the edge	20 W/m^2	60 kW/m^2	0.57 MW/m^2

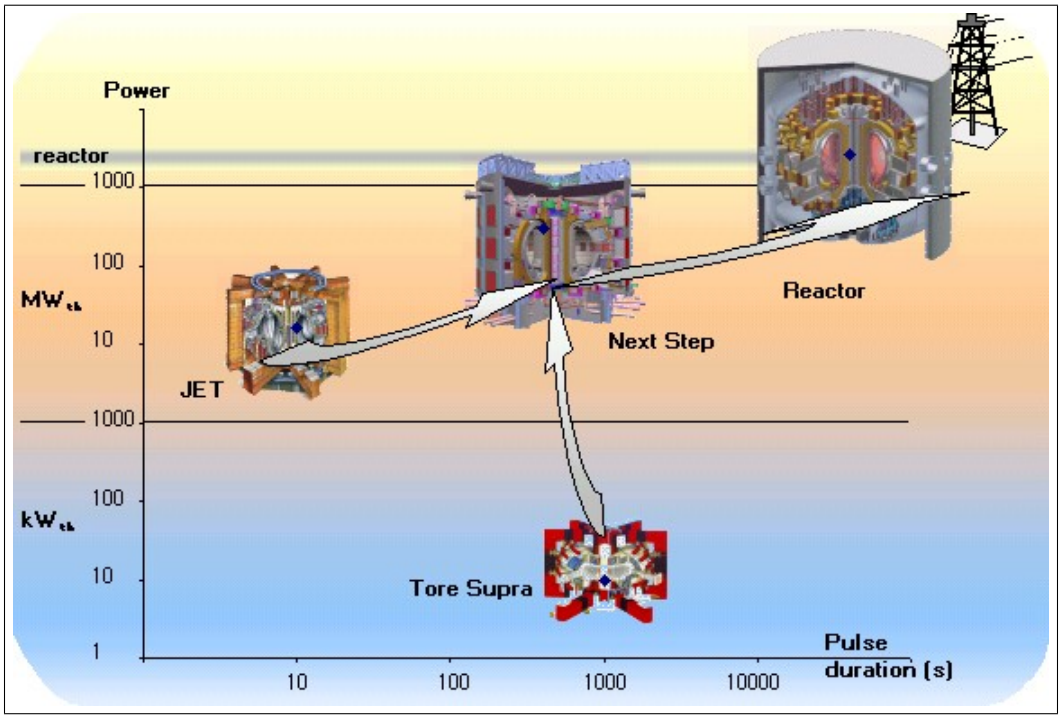

Figure C.3: TS, JET and ITER power comparative. Source: IRFM-TS

Appendix D

Edge plasma transport model and parameters **Source: The author**

During this project, three different transport equations have been used to model the particle transport in edge fusion plasmas. In this section it is expounded how the parameters for these models were obtained.

The different transport models handled in this project are:

- Diffusive model (used in the confined plasma region)

$$\frac{\delta n(x,t)}{\delta t} = D_{\perp}\frac{\delta^2 n(x,t)}{\delta r^2} + S(x,t) \tag{D.1}$$

- Diffusive model with sink term (used in the non confined plasma region or scrape off layer)

$$\frac{\delta n(x,t)}{\delta t} = D_{\perp}\frac{\delta^2 n(x,t)}{\delta r^2} - \gamma n(x,t) + S(x,t) \tag{D.2}$$

- Convective model with sink term (used in the non confined plasma region or scrape off layer)

$$\frac{\delta n(x,t)}{\delta t} + V_c\frac{\delta n(x,t)}{\delta r} = -\gamma n(x,t) + S(x,t) \tag{D.3}$$

where:

- $n(x,t)$ is the particle (electrons) density, expressed in $[particles \cdot m^3]$.
- $S(x,t)$ is the particle source that we aim to identify, expressed in $[particles \cdot m^3 \cdot s^{-1}]$.
- $D_{\perp}$ is the transversal diffusion coefficient.
- V_c is the convection coefficient.
- γ is the sink term.

Thus, we will differentiate three zones the edge plasma. To delimit the different regions, two points will be defined:

- $\mathbf{n_a}$ will mark the end of confined plasma and thus the beginning of the SOL. It will be chosen around the separatrix or LCMS (the position of the LCMS can be retrieved from the TS database for each experiment or shot).

- $\mathbf{n_b}$ will mark the beginning of the convective model in the SOL. It will be chosen around 4 cm after the LCMS

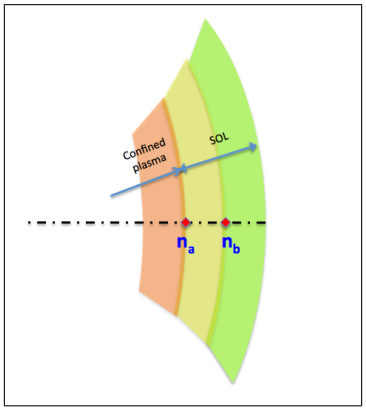

Figure D.1: Subregions in edge plasma

A The transversal diffusion coefficient $D_\perp$

The diffusion coefficient, $D_\perp$, represents the diffusion of particles (and thus, of energy) from the center of the plasma to the edge. This is a measure of the confinement quality, due to the fact that, the higher the value of $D_\perp$, the faster plasma loses its energy and thus, the worse the confinement is.

We know that the value for this parameter is around $D_\perp \approx 1m^{-2}s^{-2}$ [6]. Unfortunately, this value is quite uncertain. During this project we have used

$$D_\perp \in (0.3,\ \ 5)\ \ m^2s^{-1}$$

B The speed of convection V_c

The convection coefficient, V_c, represents, like the diffusion coefficient does, the transport of particles and energy in plasma from the center to the edge, but in this case, by convective mechanisms.

There is also a high uncertainty about the value for this parameter. Recent estimations indicates that this parameter can take values from 30 ms^{-1} to 60 ms^{-1}. This is the rank of values that has been used during this project.

$$V_c \in (30,\ \ 60)\ \ ms^{-1}$$

C The sink term γ

The sink term represents the particles and energy losses in the SOL (non-confined plasma). This losses are due to the fact that the field lines are no longer closed in the SOL. Once a particle crosses the last closed magnetic surface, it will finally escape from the plasma and be collected by the limiter or the chamber walls following one of this field lines.

Unlike the other two parameters, the sink term can be calculated with a smaller uncertainty. It can be expressed in terms of plasma and tokamaks parameters as [6]:

$$\gamma = \frac{c_s}{2L_c} \tag{D.4}$$

where c_s stands for the speed of sound in the plasma and L_c as the parallel connexion length.

C.1 Speed of sound, c_s

The speed of sound can be computed as

$$c_s = \sqrt{\frac{K(T_e + T_i)}{m}}$$

where T_e and T_i are the electron and ion temperatures and m stands for the deuterium ion mass. This mass is

$$m = 2.01355u \cdot 1.660539 \cdot 10^{-27} kg/u = 3.3436 \cdot 10^{-27} kg$$

From [13], we know that the electron temperature in the scrape-off layer is governed by the following variation law:

$$T_e = T_0 \cdot e^{r/\lambda_t} \;\; eV$$

where T_0 is the electron temperature in the LCMS (around 40 ± 5 eV), r is the distance to the last closed magnetic surface ($r \in (0,\ 0.05)$ m) and λ_T is a configuration parameter that has been taken as $\lambda_T = 0.05m$ during these experiences.

On the other hand, ion temperature is related to the electron temperature as it is sated in [13]. As a simplification, in this experiences, we have taken the ion temperature in the SOL as

$$T_i = 3T_e$$

The following plot (fig.D.2b) shows the calculated distribution for the speed of sound using the previous Te, Ti and m values.

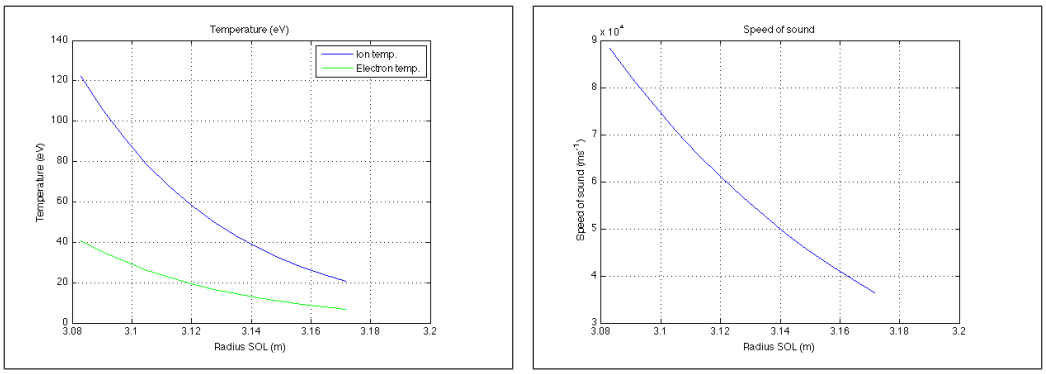

(a) Ion and electron temperatures in the SOL (b) Speed of sound in the SOL plasma

Figure D.2: Particles temperature and speed of sound in the SOL plasma

C.2 Parallel connecting length, L_c

L_c is the connexion length of the magnetic field lines and the wall or the limiter of the tokamak. When the field line finish in the limiter (fig. D.3), the connexion length can be expressed as:

$$L_c = 2\pi Rq \tag{D.5}$$

where R is the major radius of the plasma and q is the security factor, defined as the number of turns the helical magnetic field line makes around the major circumference of the tokamak (toroidal direction) per single turn of the minor circumference (poloidal direction).

In the other hand, at a given distance from the last closed magnetic surface (LCMS), the field lines don't finish in the limiter, but in the wall itself. From this distance to the end of the SOL, equation D.6 is no longer valid (field lines don't make a complete turn any longer), and the connecting length must be computed as:

$$L_c = \pi R\phi \tag{D.6}$$

where ϕ is the toroidal angle that takes to the field line to touch the wall. The poloidal angle at which the field line touches the wall is called θ, and approximately $\theta \approx 2\pi/3$ (fig. D.3).

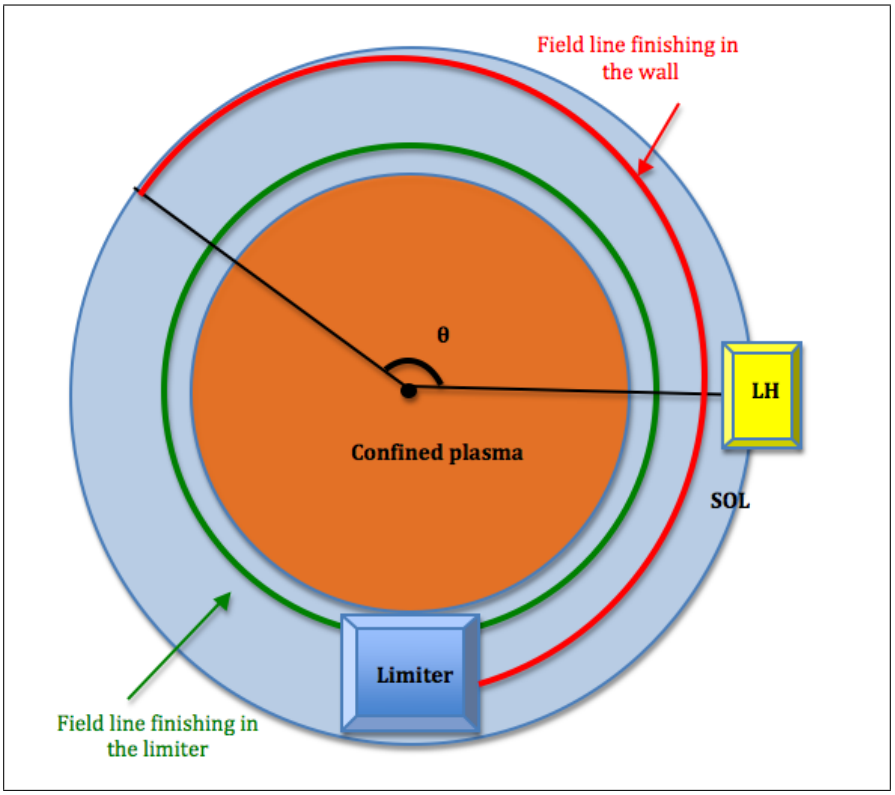

Figure D.3: Tokamak section (superposition of all sections)

Using the measurements from TS database, it is possible to retrieve the security factor and the ϕ angle. For example, for the shot TS45525, we finally obtain an estimated sink term like the one observed in figure D.4, where the $r = 3.15$ is the approximate point where we suppose that the field lines start to hit the wall.

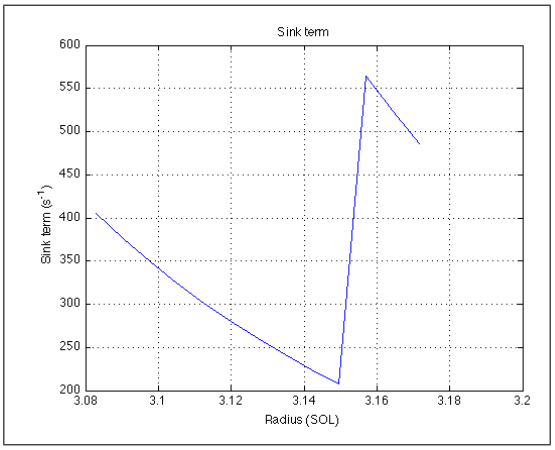

Figure D.4: Sink term for TS45525 (q=7.25 and $\theta = 5\pi$)

Appendix E

State-space representations and Extended spaces **Source: The author**

A Space discretization of the simplified transport model

Taking the simplified transport model (3.1), the following class of systems can be obtained,

$$\tilde{n}_t(x,t) = \alpha\tilde{n}_{xx}(x,t) - \gamma\tilde{n}(x,t) + S(x,t) \tag{E.1}$$

with the following boundary and initial conditions:

$$\begin{cases} \tilde{n}_x(0,t) = \tilde{n}_{x0}(t) \quad , \quad \tilde{n}(1,t) = \tilde{n}_L(t) \\ \tilde{n}(x,0) = \tilde{n}_{r0}(x) \end{cases}$$

where

- the subscripts t and x denote the time and space derivatives,
- $x = r/L \ \epsilon[0,1]$ stands for the normalized radius,
- $\alpha = D_\perp/L^2$ is the diffusion coefficient,
- $\gamma = c_s/(2L_c) > 0$ is the sink term.

Using a central discretization,

$$\frac{\delta^2 u}{\delta x^2} \approx \frac{u_{i+1} - 2u_i + u_{i-1}}{\Delta x^2} \tag{E.2}$$

if the space is split into N+1 points (N divisions), considering $\tilde{n}_1$ (corresponding to r=0) and $\tilde{n}_{N+1}$ (corresponding to r=L) as limits, the following space-discretized system of equations can be obtained for i={3, 4, ..., (N-1)}

$$\begin{aligned} \tilde{n}_{t,i}(t) &= \alpha\frac{\tilde{n}_{i+1}(t) - 2\tilde{n}_i(t) + \tilde{n}_{i-1}(t)}{\Delta x^2} - \gamma\tilde{n}_i(t) + S_i(t) = \\ &= \frac{\alpha}{\Delta x^2}\tilde{n}_{i+1}(t) - (\frac{2\alpha}{\Delta x^2} + \gamma)\tilde{n}_i(t) + \frac{\alpha}{\Delta x^2}\tilde{n}_{i-1}(t) + S_i(t) \end{aligned} \tag{E.3}$$

and using the boundary conditions (a Dirichlet condition in r=0 and a Neumann one in r=L)

$$\begin{cases} \tilde{n}_{x,0} \approx \frac{\tilde{n}_1(t)-\tilde{n}_0(t)}{\Delta x} = \tilde{n}_{x0}(t) \\ \tilde{n}_{N+1} = \tilde{n}_L(t) \end{cases} \tag{E.4}$$

the first and last equation of the system can be deduced (i=2 and i=N):

$$\begin{cases} \tilde{n}_{t,2}(t) &= \frac{\alpha}{\Delta x^2}\tilde{n}_3(t) - (\frac{\alpha}{\Delta x^2}+\gamma)\tilde{n}_2(t) - \frac{\alpha}{\Delta x}\tilde{n}_{x0}(t) + S_2(t) \\ \tilde{n}_{t,N} &= \frac{\alpha}{\Delta x^2}\tilde{n}_L(t) - (\frac{2\alpha}{\Delta x^2}+\gamma)\tilde{n}_N(t) + \frac{\alpha}{\Delta x^2}\tilde{n}_{N-1}(t) + S_N(t) \end{cases} \tag{E.5}$$

so the following system of N-1 equation yields:

$$\begin{cases} \tilde{n}_{t,2}(t) &= \frac{\alpha}{\Delta x^2}\tilde{n}_3(t) - (\frac{\alpha}{\Delta x^2}+\gamma)\tilde{n}_2(t) - \frac{\alpha}{\Delta x}\tilde{n}_{x0}(t) + S_2(t) \\ \vdots & \vdots \\ \tilde{n}_{t,i}(t) &= \frac{\alpha}{\Delta x^2}\tilde{n}_{i+1}(t) - (\frac{2\alpha}{\Delta x^2}+\gamma)\tilde{n}_i(t) + \frac{\alpha}{\Delta x^2}\tilde{n}_{i-1}(t) + S_i(t) \\ \vdots & \vdots \\ \tilde{n}_{t,N} &= \frac{\alpha}{\Delta x^2}\tilde{n}_L(t) - (\frac{2\alpha}{\Delta x^2}+\gamma)\tilde{n}_N(t) + \frac{\alpha}{\Delta x^2}\tilde{n}_{N-1}(t) + S_N(t) \end{cases} \tag{E.6}$$

B First state-space representation

From the previous obtained system (E.6), a state space representation of the form

$$\dot{\mathbf{n}} = A\mathbf{n} + B\mathbf{u} + \mathbf{w}$$

for the transport model can be deduced, where **n** is the state, **u** is the known input and **w** is a known disturbance:

$$\overbrace{\begin{pmatrix} \dot{n}_2 \\ \dot{n}_3 \\ \dot{n}_4 \\ \vdots \\ \dot{n}_i \\ \vdots \\ \dot{n}_N \end{pmatrix}}^{\dot{\mathbf{x}}}_{[N-1,1]} = \overbrace{\begin{pmatrix} a+b & a & 0 & \dots & \dots & \dots & \dots & 0 \\ a & b & a & 0 & \dots & \dots & \dots & 0 \\ 0 & a & b & a & 0 & \dots & \dots & 0 \\ \vdots & \ddots & \ddots & \ddots & \ddots & \dots & \dots & \vdots \\ 0 & \dots & a & b & a & 0 & \dots & 0 \\ \vdots & \dots & \ddots & \ddots & \ddots & \ddots & \dots & \vdots \\ 0 & \dots & \dots & \dots & \dots & 0 & a & b \end{pmatrix}}^{A}_{[N-1,N-1]} \overbrace{\begin{pmatrix} n_2 \\ n_3 \\ n_4 \\ \vdots \\ n_i \\ \vdots \\ n_N \end{pmatrix}}^{\mathbf{x}}_{[N-1,1]} +$$

$$+ \overbrace{\begin{pmatrix} 1 & 0 & \dots & \dots & 0 \\ 0 & 1 & 0 & \dots & 0 \\ \vdots & \ddots & \ddots & \dots & \vdots \\ 0 & \dots & \dots & 0 & 1 \end{pmatrix}}^{B}_{[N-1,N-1]} \overbrace{\begin{pmatrix} S_2 \\ S_3 \\ \vdots \\ S_N \end{pmatrix}}^{\mathbf{u}}_{[N-1,1]} + \overbrace{\begin{pmatrix} -\frac{\alpha}{\Delta x}n_{x0} \\ 0 \\ \vdots \\ \frac{\alpha}{\Delta x^2}n_L \end{pmatrix}}^{\mathbf{w}}_{[N-1,1]} \tag{E.7}$$

where $a = \frac{\alpha}{\Delta x^2}$ and $b = -(\frac{2\alpha}{\Delta x^2}+\gamma)$

The obtained state-space representation for the model it's suitable to use with the identification methods that are developed in this project.

C Integral action: First extended state

Since steady state error rejection is required for our estimation problem, an integral action will be introduced in the system, this means that N new states acting as integrators to the close loop system will be introduced.

$$\epsilon_{\mathbf{I}}(t) = \int (\mathbf{r}(t) - \mathbf{x}(t))dt \tag{E.8}$$

where $\mathbf{r}(t)$ stands for the desired reference, and $\mathbf{x}(t)$ is the state vector.

Thus, our extended state is now composed by another N new variables, and the extended state equation is given as :

$$\begin{aligned}\underbrace{\begin{pmatrix}\dot{\mathbf{n}}\\ \dot{\epsilon_{\mathbf{I}}}\end{pmatrix}}_{\dot{\mathbf{X}}} &= \underbrace{\begin{pmatrix}A & 0_{[N,N]}\\ -I_{[N,N]} & 0_{[N,N]}\end{pmatrix}}_{A_e}\underbrace{\begin{pmatrix}\mathbf{n}\\ \epsilon_{\mathbf{I}}\end{pmatrix}}_{\mathbf{X}} + \underbrace{\begin{pmatrix}I_{[N,N]}\\ 0_{[N,N]}\end{pmatrix}}_{B_{e_1}}\mathbf{S}\\ &+ \underbrace{\underbrace{\begin{pmatrix}-\frac{\alpha}{\Delta x} & 0 & 0 & \dots & \dots & 0\\ 0 & 0 & 0 & \dots & \dots & 0\\ \vdots & \vdots & \vdots & \dots & \dots & \vdots\\ 0 & \frac{\alpha}{\Delta x^2} & 0 & \dots & \dots & 0\\ 0 & 0 & 1 & 0 & \dots & 0\\ \vdots & \vdots & 0 & 1 & \dots & 0\\ \vdots & \vdots & \vdots & \dots & \ddots & 0\\ 0 & 0 & 0 & \dots & \dots & 1\end{pmatrix}}_{B_{e_2}}\underbrace{\begin{pmatrix}n_{x0}\\ n_L\\ n_{m_1}\\ n_{m_2}\\ \vdots\\ n_{m_N}\end{pmatrix}}_{\mathbf{\Omega}}}_{\mathbf{w}}\end{aligned} \tag{E.9}$$

that is,

$$\underbrace{\dot{\mathbf{X}}(t)}_{[2N,1]} = \underbrace{A_e}_{[2N,2N]}\underbrace{\mathbf{X}(t)}_{[2N,1]} + \underbrace{B_{e_1}}_{[2N,N]}\underbrace{\mathbf{S}(t)}_{[N,1]} + \underbrace{\mathbf{w}(t)}_{[2N,1]}$$

Now, we will apply the problem studied in section **??** to this extended state to obtained the so-called optimal source.

D Second extended state: Time varying boundary conditions

We can take advantage of the fact that the reference density (the measurement data) is known in advance. That means that we already know the boundary conditions that we want our tracked density to satisfy for each instant.

$$n_{x0}(t) = \frac{n_{m_2}(t) - n_{m_1}(t)}{\Delta x} \tag{E.10}$$

$$n_L = n_{m_{100}} \tag{E.11}$$

Then, we realize that the boundary conditions can be "introduced" in the system (E.9). Rewriting the previous system we have:

$$\underbrace{\begin{pmatrix}\dot{\mathbf{n}}\\ \dot{\epsilon_{\mathbf{I}}}\end{pmatrix}}_{\dot{\mathbf{X}}} = \underbrace{\begin{pmatrix}A & 0_{[N,N]}\\ -I_{[N,N]} & 0_{[N,N]}\end{pmatrix}}_{A_e}\underbrace{\begin{pmatrix}\mathbf{n}\\ \epsilon_{\mathbf{I}}\end{pmatrix}}_{\mathbf{X}} + \underbrace{\begin{pmatrix}I_{[N,N]}\\ 0_{[N,N]}\end{pmatrix}}_{B_{e_1}}\mathbf{S}$$

$$+\underbrace{\underbrace{\begin{pmatrix}-\frac{\alpha}{\Delta x} & 0 & 0 & \dots & \dots & 0\\ 0 & 0 & 0 & \dots & \dots & 0\\ \vdots & \vdots & \vdots & \dots & \dots & \vdots\\ 0 & \frac{\alpha}{\Delta x^2} & 0 & \dots & \dots & 0\\ 0 & 0 & 1 & 0 & \dots & 0\\ \vdots & \vdots & 0 & 1 & \dots & 0\\ \vdots & \vdots & \vdots & \dots & \ddots & 0\\ 0 & 0 & 0 & \dots & \dots & 1\end{pmatrix}}_{B_{e_2}}\underbrace{\begin{pmatrix}n_{x0}\\ n_L\\ n_{m_1}\\ n_{m_2}\\ \vdots\\ n_{m_N}\end{pmatrix}}_{\mathbf{\Omega}}}_{\mathbf{w}}$$

and taking into account (E.10) and (E.11) we can write the system as:

$$\underbrace{\begin{pmatrix}\dot{\mathbf{n}}\\ \dot{\epsilon_{\mathbf{I}}}\end{pmatrix}}_{\dot{\mathbf{X}}} = \underbrace{\begin{pmatrix}A & 0_{[N,N]}\\ -I_{[N,N]} & 0_{[N,N]}\end{pmatrix}}_{A_e}\underbrace{\begin{pmatrix}\mathbf{n}\\ \epsilon_{\mathbf{I}}\end{pmatrix}}_{\mathbf{X}} + \underbrace{\begin{pmatrix}I_{[N-1,N-1]}\\ 0_{[N-1,N-1]}\end{pmatrix}}_{B_{e_1}}\mathbf{S}$$

$$+\underbrace{\underbrace{\begin{pmatrix}\frac{\alpha}{\Delta x^2} & -\frac{\alpha}{\Delta x^2} & 0 & \dots & \dots & 0\\ 0 & 0 & 0 & \dots & \dots & 0\\ \vdots & \vdots & \vdots & \dots & \dots & \vdots\\ 0 & 0 & 0 & \dots & \dots & \frac{\alpha}{\Delta x^2}\\ 1 & 0 & 0 & \dots & 0 & 0\\ 0 & 1 & 0 & \dots & 0 & \vdots\\ \vdots & \dots & \ddots & \dots & 0 & \vdots\\ 0 & 0 & 0 & \dots & 1 & 0\end{pmatrix}}_{B_{e_2}}\underbrace{\begin{pmatrix}n_{m_1}\\ n_{m_2}\\ n_{m_3}\\ \vdots\\ n_{m_N+1}\end{pmatrix}}_{\mathbf{n_m}}}_{\mathbf{w}} \tag{E.12}$$

Now, the vector $\mathbf{w}(t)$ takes into account the boundary condition, so we don't have constant boundary conditions anymore.

E State-space from linearized constrained system

To introduce the gaussian constraint to the input, we will impose in the model equations (E.6) a gaussian shaped source:

$$\begin{cases} \tilde{n}_{t,1}(t) = \frac{\alpha}{\Delta x^2}\tilde{n}_2(t) - (\frac{\alpha}{\Delta x^2}+\gamma)\tilde{n}_1(t) - \frac{\alpha}{\Delta x}\tilde{n}_{x0}(t) + \overbrace{\sum_{j=l,LH}\theta_j(t)e^{-(x_1-\mu_j(t))^2/(2\sigma_j(t)^2)}}^{S_1(t)} \\ \vdots \\ \tilde{n}_{t,i}(t) = \frac{\alpha}{\Delta x^2}\tilde{n}_{i+1}(t) - (\frac{2\alpha}{\Delta x^2}+\gamma)\tilde{n}_i(t) + \frac{\alpha}{\Delta x^2}\tilde{n}_{i-1}(t) + \overbrace{\sum_{j=l,LH}\theta_j(t)e^{-(x_i-\mu_j(t))^2/(2\sigma_j(t)^2)}}^{S_i(t)} \\ \vdots \\ \tilde{n}_{t,N} = \frac{\alpha}{\Delta x^2}\tilde{n}_L(t) - (\frac{2\alpha}{\Delta x^2}+\gamma)\tilde{n}_N(t) + \frac{\alpha}{\Delta x^2}\tilde{n}_{N-1}(t) + \overbrace{\sum_{j=l,LH}\theta_j(t)e^{-(x_N-\mu_j(t))^2/(2\sigma_j(t)^2)}}^{S_N(t)} \end{cases} \tag{E.13}$$

As input variable we won't have the S(t) vector anymore, but the vector ϑ, defined as:

$$\vartheta(t) = \begin{pmatrix} \theta_l(t) \\ \mu_l(t) \\ \sigma_l(t) \\ \theta_{LH}(t) \\ \mu_{LH}(t) \\ \sigma_{LH}(t) \end{pmatrix} \tag{E.14}$$

Thus, the dimension of the input vector has decreased from $[N, 1]$ to $[6, 1]$.

The problem now is that the system with the constrained input is no longer linear with respect to the chosen input ϑ(t) (notice that the previous system was already linear with respect to the input $\mathbf{S}$(t)). Therefore, we must linearize the system around an equilibrium point.
Then, the linearized system around the equilibrium point (designated by the subindex 'eq'), remains:

$$\overbrace{\begin{pmatrix} \Delta\dot{n}_1 \\ \Delta\dot{n}_2 \\ \Delta\dot{n}_3 \\ \vdots \\ \Delta\dot{n}_i \\ \vdots \\ \Delta\dot{n}_N \end{pmatrix}}^{\mathbf{\Delta\dot{n}}} = \overbrace{\begin{pmatrix} a+b & a & 0 & \dots & \dots & \dots & \dots & 0 \\ a & b & a & 0 & \dots & \dots & \dots & 0 \\ 0 & a & b & a & 0 & \dots & \dots & 0 \\ \vdots & \ddots & \ddots & \ddots & \ddots & \dots & \dots & \vdots \\ 0 & \dots & a & b & a & 0 & \dots & 0 \\ \vdots & \dots & \ddots & \ddots & \ddots & \ddots & \dots & \vdots \\ 0 & \dots & \dots & \dots & \dots & 0 & a & b \end{pmatrix}}^{A_c \equiv A} \overbrace{\begin{pmatrix} \Delta n_1 \\ \Delta n_2 \\ \Delta n_3 \\ \vdots \\ \Delta n_i \\ \vdots \\ \Delta n_N \end{pmatrix}}^{\mathbf{\Delta n}} +$$

$$+\nabla\mathbf{S}|_{eq} \underbrace{\begin{pmatrix} \Delta\theta_l \\ \Delta\mu_l \\ \Delta\sigma_l \\ \Delta\theta_{LH} \\ \Delta\mu_{LH} \\ \Delta\sigma_{LH} \end{pmatrix}}_{\mathbf{\Delta}\vartheta(t)} + \underbrace{\begin{pmatrix} -\frac{\alpha}{\Delta x}\Delta n_{x0}(t) \\ 0 \\ \vdots \\ \frac{\alpha}{\Delta x^2}\Delta n_L(t) \end{pmatrix}}_{\mathbf{\Delta bc}(t)} \tag{E.15}$$

where

- $a = \frac{\alpha}{\Delta x^2}$
- $b = -(\frac{2\alpha}{\Delta x^2} + \gamma)$
- $\nabla \mathbf{S}|_{eq} = \begin{pmatrix} \frac{\delta S_l}{\delta \theta_l}|_{x_1} & \frac{\delta S_l}{\delta \mu_l}|_{x_1} & \frac{\delta S_l}{\delta \sigma_l}|_{x_1} & \frac{\delta S_{LH}}{\delta \theta_{LH}}|_{x_1} & \frac{\delta S_{LH}}{\delta \mu_{LH}}|_{x_1} & \frac{\delta S_{LH}}{\delta \sigma_{LH}}|_{x_1} \\ \vdots & \vdots & \vdots & \vdots & \vdots & \vdots \\ \frac{\delta S_l}{\delta \theta_l}|_{x_N} & \frac{\delta S_l}{\delta \mu_l}|_{x_N} & \frac{\delta S_l}{\delta \sigma_l}|_{x_N} & \frac{\delta S_{LH}}{\delta \theta_{LH}}|_{x_N} & \frac{\delta S_{LH}}{\delta \mu_{LH}}|_{x_N} & \frac{\delta S_{LH}}{\delta \sigma_{LH}}|_{x_N} \end{pmatrix} \Bigg|_{eq}$

E.1 Equilibrium source

To calculate the equilibrium point we solve the system of equations (E.13) when the condition $\dot{\mathbf{n}}(t) = 0$ is applied. The following overdetermined system of equations yelds:

$$\mathbf{0} = \overbrace{\begin{pmatrix} a+b & a & 0 & \dots & \dots & \dots & \dots & 0 \\ a & b & a & 0 & \dots & \dots & \dots & 0 \\ 0 & a & b & a & 0 & \dots & \dots & 0 \\ \vdots & \ddots & \ddots & \ddots & \ddots & \dots & \dots & \vdots \\ 0 & \dots & a & b & a & 0 & \dots & 0 \\ \vdots & \dots & \ddots & \ddots & \ddots & \ddots & \dots & \vdots \\ 0 & \dots & \dots & \dots & \dots & 0 & a & b \end{pmatrix}}^{A} \overbrace{\begin{pmatrix} n_{1,eq} \\ n_{2,eq} \\ n_{3,eq} \\ \vdots \\ n_{i,eq} \\ \vdots \\ n_{N,eq} \end{pmatrix}}^{\mathbf{n_{eq}}} +$$

$$+ \overbrace{\begin{pmatrix} \sum_{j=l,LH} \left(\theta_{j,eq} e^{-(x_1 - \mu_{j,eq})^2/(2\sigma_{j,eq})} \right) \\ \sum_{j=l,LH} \left(\theta_{j,eq} e^{-(x_2 - \mu_{j,eq})^2/(2\sigma_{j,eq})} \right) \\ \vdots \\ \sum_{j=l,LH} \left(\theta_{j,eq} e^{-(x_{(N-1)} - \mu_{j,eq})^2/(2\sigma_{j,eq})} \right) \\ \sum_{j=l,LH} \left(\theta_{j,eq} e^{-(x_{(N)} - \mu_{j,eq})^2/(2\sigma_{j,eq})} \right) \end{pmatrix}}^{S_{eq}} + \overbrace{\begin{pmatrix} -\frac{\alpha}{\Delta x} n_{x0,eq} \\ 0 \\ \vdots \\ 0 \\ +\frac{\alpha}{\Delta x^2} n_{L,eq}^2 \end{pmatrix}}^{W_{eq}} \tag{E.16}$$

As it can be seen, the previous system of equations is an overdetermined system, with $[N-1]$ equations and $[N+7]$ undetermined variables:

$$[\underbrace{n_{1,eq}, n_{2,eq}, ..., n_{N,eq}}_{\mathbf{n_{eq}}_{[N]}}, \underbrace{\theta_{l,eq}, \mu_{l,eq}, \sigma_{l,eq}, \theta_{LH,eq}, \mu_{LH,eq}, \sigma_{LH,eq}}_{\vartheta_{\mathbf{eq}[6]}}, \underbrace{n_{x0,eq}, n_{L,eq}}_{\mathbf{bc_{eq}}_{[2]}}]$$

To solve this system, 8 variables could be set in order to have a determined system (N equations and N undetermined). Numeric values could be assigned to the equilibrium input vector (i.e. $\vartheta_{\mathbf{eq}[6]}$) and the equilibrium boundary conditions (i.e. $\mathbf{bc_{eq}}_{[2]}$) and then, the values for the equilibrium density vector ($\mathbf{n_{eq}}_{[N]}$) would be obtained. But this would be an inaccurate method. A more convenient method to calculate the equilibrium point consists in using an observer to estimate the source term such that minimizes the deviation, ϵ, from the equilibrium point :

$$\epsilon(\vartheta) = A\mathbf{n_{eq}} + \mathbf{W_{eq}} + S(\vartheta) \tag{E.17}$$

where $\mathbf{n_{eq}}$ is chosen as the mean density in a time period in which the LH antenna is on (fig.E.1), $\mathbf{W_{eq}}$ is computed using the mean boundary conditions in the interval, and ϑ is the set of optimal parameters for the gaussian source that we want to find.

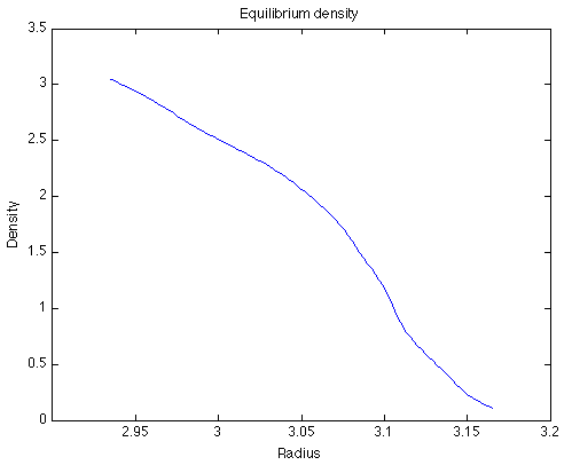

Figure E.1: Mean density distribution when LH antenna is on

To find the optimal set of variables ϑ, we study the dynamics of the following expression:

$$\dot{\epsilon(\vartheta)} + \lambda\epsilon(\vartheta) = 0 \tag{E.18}$$

From this differential equation it yields:

$$\epsilon = e^{-\lambda p} \to 0$$

where p is the integration step and λ is a tuning parameter. Then, the following iterative expression yields to compute the optimal set of variables ϑ_{eq}:

$$\vartheta_{eq}^{k+1} = \vartheta_{eq}^{k} - \Delta p \left(S^{\dagger}(\vartheta_{eq}^{k})^{-1} \lambda \left(A\mathbf{n_{eq}} + \mathbf{W_{eq}} + S(\vartheta_{eq}^{k}) \right) \right) \tag{E.19}$$

F State space from the 3-models system

Integrating the three transport models (see appendix D) in the same system, the following state-space representation yields:

$$
\overbrace{\begin{pmatrix} \dot{n}_2 \\ \dot{n}_3 \\ \dot{n}_4 \\ \vdots \\ \dot{n}_{a-1} \\ \dot{n}_a \\ \dot{n}_{a+1} \\ \vdots \\ \dot{n}_{b-1} \\ \dot{n}_b \\ \dot{n}_{b+1} \\ \vdots \\ \dot{n}_N \end{pmatrix}}^{\dot{\mathbf{x}}}_{[N-1,1]} =
\overbrace{\begin{pmatrix}
a1+a2 & a3 & 0 & \dots & \dots & \dots & \dots & \dots & \dots & \dots & \dots & 0 \\
a1 & a2 & a3 & 0 & \dots & \dots & \dots & \dots & \dots & \dots & \dots & 0 \\
0 & a1 & a2 & a3 & 0 & \dots & \dots & \dots & \dots & \dots & \dots & 0 \\
\vdots & \ddots & \ddots & \ddots & \ddots & \dots & \dots & \dots & \dots & \dots & \dots & \vdots \\
0 & \dots & a1 & a2 & a3 & 0 & 0 & \dots & \dots & \dots & \dots & 0 \\
0 & \dots & 0 & b1 & b2 & b3 & 0 & \dots & \dots & \dots & \dots & 0 \\
0 & \dots & 0 & 0 & b1 & b2 & b3 & \dots & \dots & \dots & \dots & 0 \\
\vdots & \dots & \ddots & \ddots & \ddots & \ddots & \ddots & \dots & \dots & \dots & \dots & \vdots \\
0 & \dots & \dots & \dots & \dots & b1 & b2 & b3 & 0 & 0 & \dots & 0 \\
0 & \dots & \dots & \dots & \dots & 0 & b1+c1 & b2+c2 & b3 & 0 & \dots & 0 \\
0 & \dots & \dots & \dots & \dots & 0 & 0 & b1+c1 & b2+c2 & b3 & \dots & 0 \\
\vdots & \dots & \dots & \dots & \dots & \ddots & \ddots & \ddots & \ddots & \ddots & \dots & \vdots \\
0 & \dots & \dots & \dots & \dots & \dots & \dots & \dots & \dots & \dots & b1+c1 & b2+c2+b3
\end{pmatrix}}^{A}_{[N-1,N-1]}
\overbrace{\begin{pmatrix} n_2 \\ n_3 \\ n_4 \\ \vdots \\ n_{a-1} \\ n_a \\ n_{a+1} \\ \vdots \\ n_{b-1} \\ n_b \\ n_{b+1} \\ \vdots \\ n_N \end{pmatrix}}^{\mathbf{x}}_{[N-1,1]}
$$

$$
+ \overbrace{\begin{pmatrix} 1 & 0 & \dots & \dots & 0 \\ 0 & 1 & 0 & \dots & 0 \\ \vdots & \ddots & \ddots & \dots & \vdots \\ 0 & \dots & \dots & 0 & 1 \end{pmatrix}}^{B}_{[N-1,N-1]}
\overbrace{\begin{pmatrix} S_2 \\ S_3 \\ \vdots \\ S_N \end{pmatrix}}^{\mathbf{u}}_{[N-1,1]}
+ \overbrace{\begin{pmatrix} -\frac{\alpha}{\Delta x} n_{x0} \\ 0 \\ \vdots \\ \frac{\alpha}{\Delta x^2} n_L \end{pmatrix}}^{\mathbf{w}}_{[N-1,1]} \tag{E.20}
$$

where

- $a_{1,i} = a_{3,i} = Da_i/\Delta x^2$ and $a_{2,i} = -2Da_i/\Delta x^2$
- $b_{1,i} = b_{3,i} = Db_i/\Delta x^2$ and $b_{2,i} = -(2Db_i/\Delta x^2 + \gamma_i)$
- $c_{1,i} = Vc_i/\Delta x$ and $c_{2,i} = -(Vc_i/\Delta x + \gamma_i)$

It must be noticed that now, with this new state space,it is also possible to include space varying parameters for $D_\perp$, Vc and γ.

The obtention of the expanded state is analogous to the obtention of the time-varying boundary conditions extended state in the section of this appendix.

Appendix F

Optimal tracking problem and algebraic approach

A Generalized optimal tracking problem Source: [10]

Let's consider a controllable and observable system:

$$\begin{cases} \overbrace{\dot{\mathbf{x}} = A\mathbf{x} + B\mathbf{u}}^{\mathbf{f}(\mathbf{x},\mathbf{u})} \\ \mathbf{y} = C\mathbf{x} \end{cases} \tag{F.1}$$

with initial condition $\mathbf{x}(0) = \mathbf{0}$.

Lets consider a vector of reference variables $\mathbf{r}$(t) (the variables that the output variables must follow). Defining the error vector $\mathbf{e}$(t) as:

$$\mathbf{e}(t) = \mathbf{r}(t) - \mathbf{y}(t) \tag{F.2}$$

then, we can say that our aim is to control the system so that this error vector will be close to zero.

We define now our cost function as:

$$J = \underbrace{\frac{1}{2}\mathbf{e}^T(t_f)Q_{t_f}\mathbf{e}(t_f)}_{G_{t_f}} + \frac{1}{2}\int_0^{t_f} \underbrace{(\mathbf{e}^T(t)Q\mathbf{e}(t) + \mathbf{u}(t)^T R\mathbf{u}(t))}_{F}\, dt \tag{F.3}$$

where

- Q_{t_f} is a real symetric positive semidefinite matrix,
- Q is a real symetric positive semidefinite matrix,
- R is a real symetric positive definite matrix.

Lets define the Hamiltonian as:

$$H = F + \lambda^{\mathbf{T}}(t) f(\mathbf{x}, \mathbf{u}) = \frac{1}{2}(\mathbf{e}^T(t) Q \mathbf{e}(t) + \mathbf{u}(t) R \mathbf{u}(t)) + \lambda^{\mathbf{T}}(t)(A\mathbf{x} + B\mathbf{u}) \tag{F.4}$$

where λ(t) is the adjoint vector, that is supposed to verify:

$$\frac{d\lambda}{dt} = -\frac{\delta H}{\delta \mathbf{x}} = C^T Q(\mathbf{r}(t) - C\mathbf{x}(t)) - A^T \lambda(t) \tag{F.5}$$

with the final condition:

$$\lambda(t_f) = (\frac{\delta G_{t_f}}{\delta \mathbf{x}})_{t_f} \tag{F.6}$$

Then, it can be proved that the necessary condition for optimality (minimum) reads:

$$\frac{\delta H}{\delta \mathbf{u}} = 0 \tag{F.7}$$

Using this optimality principle, $\mathbf{u}$(t) can be expressed as

$$\mathbf{u}(t) = -R^{-1} B^T \lambda(t) \tag{F.8}$$

It can also be shown that:

$$\lambda(t) = P(t)\mathbf{x}(t) - \gamma_{\mathbf{d}}(t) \tag{F.9}$$

from where yields:

$$\frac{d\lambda}{dt} = \dot{P}(t)\mathbf{x}(t) + P(t)\dot{\mathbf{x}}(t) - \dot{\gamma_d}(t) \tag{F.10}$$

Substituting $\mathbf{u}$ and $\lambda(t)$ from (F.8) and (F.9) into the state equation (F.1)

$$\dot{\mathbf{x}}(t) = A\mathbf{x}(t) - BR^{-1}B^T P(t)\mathbf{x}(t) + BR^{-1}B^T \gamma_d(t) \tag{F.11}$$

Thus, equation(F.10) can also be written as:

$$\frac{d\lambda}{dt} = [\dot{P}(t) + P(t)A - P(t)BR^{-1}B^T P(t)]\mathbf{x}(t) + P(t)BR^{-1}B^T \gamma_d(t) - \dot{\gamma_d}(t) \tag{F.12}$$

or substituting (F.9) in (F.5)

$$\frac{d\lambda}{dt} = [-C^T QC - A^T P(t)]\mathbf{x}(t) + A^T \gamma_d(t) + C^T Q\mathbf{r}(t) \tag{F.13}$$

Since these two equations ((F.12) and (F.13)) hold for any $\mathbf{x}$(t) and $\mathbf{r}$(t) (if the optimal solution exists), then, the P matrix and the $\gamma_d(t)$ vector satisfy the following differential equations:

$$\dot{P}(t) = -P(t)A - A^T P(t) + P(t)BR^{-1}B^T P(t) - C^T QC \tag{F.14}$$

$$\dot{\gamma_d}(t) = [P(t)BR^{-1}B^T - A^T]\gamma_d(t) - C^T Q\mathbf{r}(t) \tag{F.15}$$

where the final conditions can be obtained from (F.6) and (F.9)

$$P(t_f) = C^T Q_{t_f} C \tag{F.16}$$

$$\gamma_d(t_f) = C^T Q_{t_f} \mathbf{r}(t_f) \tag{F.17}$$

Considering that $\mathbf{u}(t) = -R^{-1}B^T\lambda(t)$, we can finally say that the optimal input is:

$$\mathbf{u}(t) = -R^{-1}B^T\lambda(t) = -R^{-1}B^T(P(t)\mathbf{x}(t) - \gamma_{\mathbf{d}}(t))$$

So, the problem now consists in solving equations (F.14) and (F.15)

B Algebraic approach solution **Source: The author**

Solving equations (F.14) and (F.15) is not a trivial problem. But if infinite final time conditions are supposed ($t_f = \infty$), It can be shown that

$$\dot{P}(t) = 0$$

We will also take in this chapter the following algebraic approximation:

$$\dot{\gamma}(t) = 0$$

Then, with this two approximations, equations (F.14) and (F.15) can be solved.

$$PA_e + A_e^T P - PB_{e_1}R^{-1}B_{e_1}^T P = -Q \tag{F.18}$$

$$\gamma = [PB_{e_1}R^{-1}B_{e_1}^T - A_e^T]^{-1}P\underbrace{B_{e_2}\mathbf{\Omega}(t)}_{\mathbf{w}(t)} \tag{F.19}$$

The first equation (F.18) is an algebraic Ricatti equation from where P can be obtained. Once P has been calculated, we can straightly obtain γ from equation (F.19).

The optimal input $\mathbf{S}$(t) is thus,

$$\begin{aligned}\mathbf{S}(t) = -R^{-1}B_{e1}^T\lambda(t) = -R^{-1}B_{e1}^T[P(t)\mathbf{X}(t) + \gamma(t)] = \\ = \mathbf{S}(t) = \underbrace{-R^{-1}B_{e_1}^T P}_{G_{lqr}}\mathbf{X}(t)\underbrace{-R^{-1}B_{e_1}^T[PB_{e_1}R^{-1}B_{e_1}^T - A_e^T]^{-1}PB_{e_2}}_{G_w}\mathbf{\Omega}(t)\end{aligned} \tag{F.20}$$

Then, under the quasi steady state hypothesis, the optimal tracking structure for our estimation problem can be written as shown in (fig.F.1)

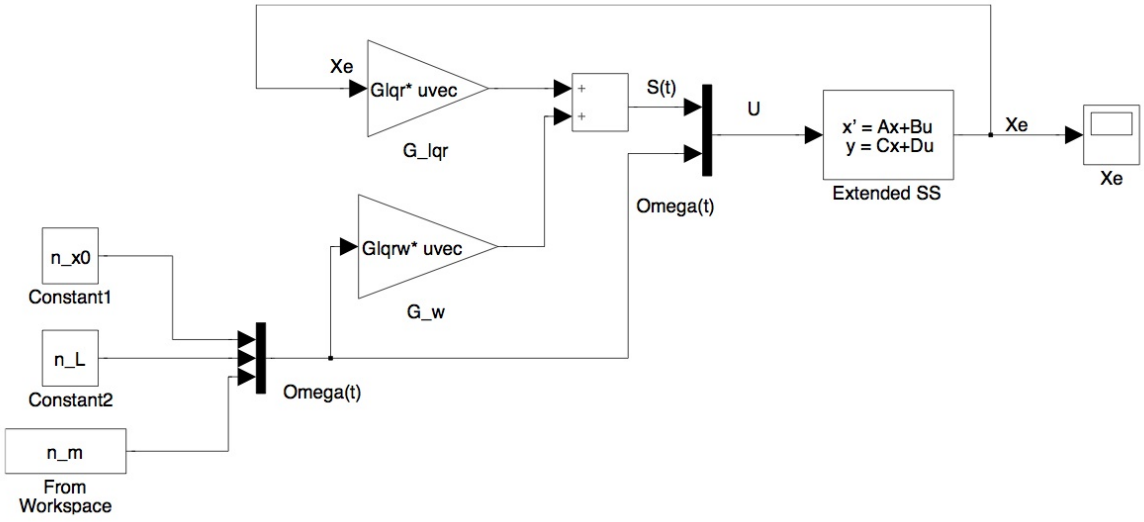

Figure F.1: Tracking structure

where the extended state space equation is now expressed as

$$\dot{\mathbf{X}}(t) = A_e\mathbf{X}(t) + \underbrace{\begin{pmatrix} B_{e_1} & B_{e_2} \end{pmatrix}}_{B_e} \underbrace{\begin{pmatrix} \mathbf{S}(t) \\ \mathbf{\Omega}(t) \end{pmatrix}}_{\mathbf{U}(t)} \tag{F.21}$$

Appendix G

Estimation theorem. Online estimation structure

A Estimation theorem Source: [14]

Consider the general class of systems described as

$$\begin{cases} n_t = \mathcal{A}(n, n_{xx}, u)\vartheta \\ a_1 n_x(0,t) + a_2 n(0,t) = a_3 \\ a_4 n_x(L,t) + a_5 n(L,t) = a_6 \end{cases} \tag{G.1}$$

where n is the state, u is a known exogenous input, $\vartheta \in \mathbb{R}^M$ stands for a set of time-varying parameters, $\mathcal{A}(n, n_{xx}, u) \in \mathbb{R}^{1xM}$ denotes the input-to-state relationship and a_i are scalar real coefficients.

The estimated state $\hat{n}(x,t)$ converges exponentially to $p(x,t)$ with:

$$||n(x,t) - \hat{n}(x,t)||_2^2 = e^{-2(\beta+\lambda)t}||n(x,0) - \hat{n}(x,0)||_2^2$$

where β and λ are positive scalar parameters, if:

$$\begin{cases} \hat{n}_t = \mathcal{A}(\hat{n}, \hat{n}_{xx}, u)\hat{\vartheta} + \beta(n - \hat{n}) \\ a_1 \hat{n}_x(0,t) + a_2 \hat{n}(0,t) = a_3 \\ a_4 \hat{n}_x(L,t) + a_5 \hat{n}(L,t) = a_6 \end{cases} \tag{G.2}$$

where $\hat{\vartheta}$ can be computed as:

$$\hat{\vartheta} = \mathcal{A}(\hat{n}, \hat{n}_{xx}, u)^{\dagger}[n_t + \lambda(n - \hat{n})] \tag{G.3}$$

where $A^{\dagger}$ stands for the Moore-Penrose pseudo inverse of A. β and λ are the tuning parameters for the estimator, and they must be set in order to control the convergence of the estimated dynamics and to moderate the variations of $\hat{\vartheta}$.

B Application of the theorem: Online estimation structure **Source: The author**

In our particular case, our system can be written as

$$\begin{cases} n_t = \overbrace{[n(t), n_{xx}(t), u(t)]}^{\mathcal{A}} \overbrace{[\alpha(t), \gamma(t), s(t)]'}^{\vartheta} \\ n_x(0,t) = n_{x0} \\ n(L,t) = n_L \end{cases} \tag{G.4}$$

and since our system has been space-discretized in N points, it can be expressed as:

$$\begin{pmatrix} \dot{n_1}(t) \\ \vdots \\ \dot{n_i}(t) \\ \vdots \\ \dot{n_N}(t) \end{pmatrix} = \begin{pmatrix} \frac{1}{\Delta x^2}(n_2(t) - n_1(t) - \Delta x n_{x0}(t)) & n_1(t) & S_1(t) \\ \vdots & \vdots & \vdots \\ \frac{1}{\Delta x^2}(n_{i+1}(t) - 2n_i(t) + n_{i-1}(t)) & n_i(t) & S_i(t) \\ \vdots & \vdots & \vdots \\ \frac{1}{\Delta x^2}(n_L(t) - 2n_N(t) + n_{N-1}(t)) & n_N(t) & S_N(t) \end{pmatrix} \begin{pmatrix} \alpha(t) \\ \gamma(t) \\ s(t) \end{pmatrix} \tag{G.5}$$

To implement the estimator obtained in this theorem, the system must be time discretized. Using a sampling time t_s, our system can be discretized as:

$$\begin{pmatrix} n_1^{k+1} \\ \vdots \\ n_i^{k+1} \\ \vdots \\ n_N^{k+1} \end{pmatrix} = \begin{pmatrix} n_1^k \\ \vdots \\ n_i^k \\ \vdots \\ n_N^k \end{pmatrix} + t_s \begin{pmatrix} \frac{1}{\Delta x^2}(n_2^k - n_1^k - \Delta x n_{x0}^k) & n_1^k & S_1^k \\ \vdots & \vdots & \vdots \\ \frac{1}{\Delta x^2}(n_{i+1}^k - 2n_i^k + n_{i-1}^k) & n_i^k & S_i^k \\ \vdots & \vdots & \vdots \\ \frac{1}{\Delta x^2}(n_L^k - 2n_N^k + n_{N-1}^k) & n_N^k & S_N^k \end{pmatrix} \begin{pmatrix} \alpha \\ \gamma \\ s \end{pmatrix} \tag{G.6}$$

C Estimation structure verification. **Source: The author**

In this section, the performance of the estimation structure will be tested.

A theoretical Gaussian source multiplied by a sinus will be introduced in the model. Both, the theoretical distributed gaussian source and the obtained density will be introduced in the structure as inputs. Then, we will check if the estimated coeficients, $\hat{\vartheta}$, take the same values. The verification scheme can be seen in (fig.G.1)

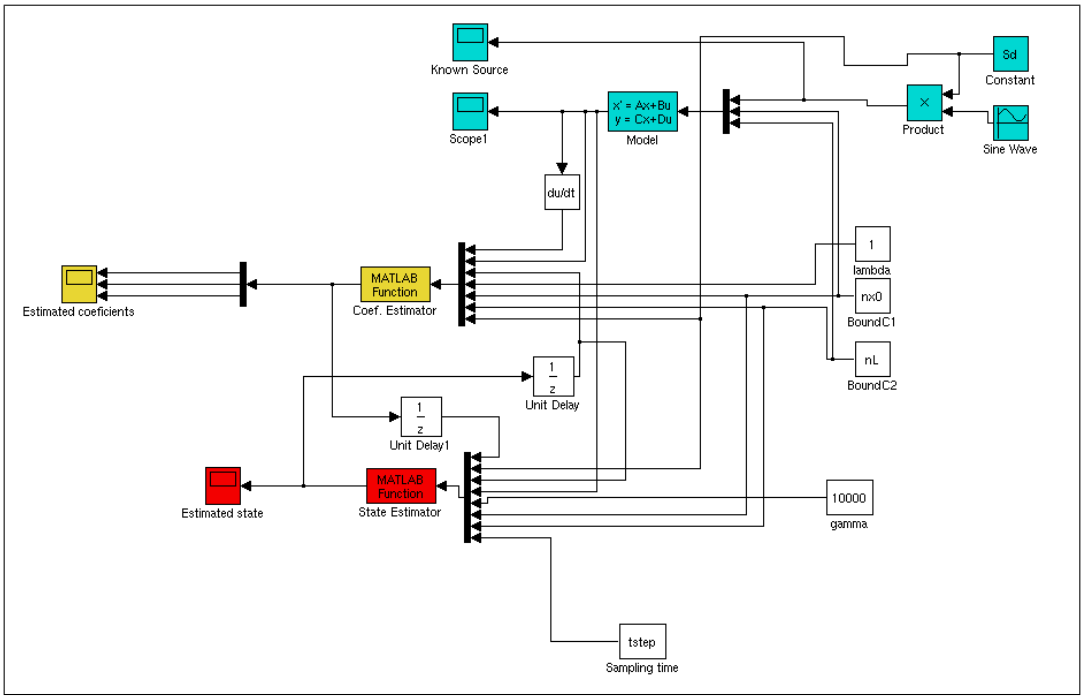

Figure G.1: Online estimation structure

The coefficients introduced in the model to generate the density (in blue in fig.G.1) are:

- $\alpha = 18.5432$
- $\gamma = -30.5427$
- s(t) is a sinusoidal function centered in y=1 and with amplitude A=1.

The boundary conditions introduced as input to the state and parameter identification are the same that the introduced in the model to generate de theoretical density:

- $n_{x0} = -0.04$
- $n_L = 0.005$

the tuning parameters for the estimator are chosen in order to obtain a fast convergence for the estimated density

- $\lambda = 1$
- $\beta = 1000$

Finally, the sampling time is chosen as $t_s = 10^{-6}$

The shape of the introduced source and density are shown in (fig.G.2)

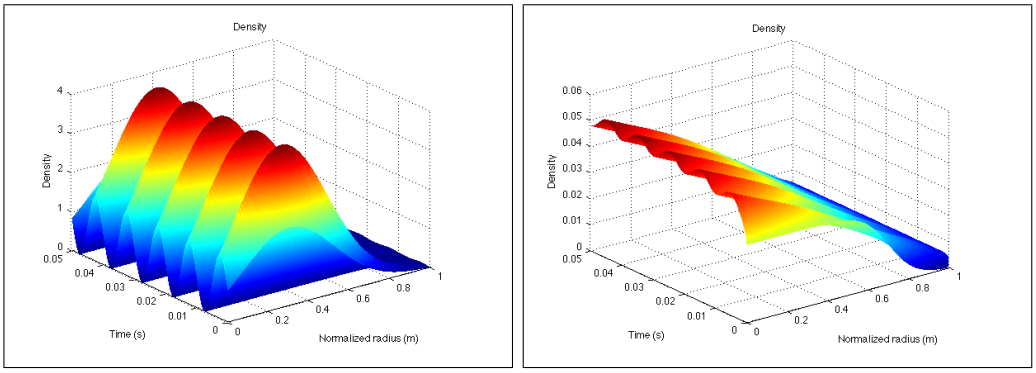

(a) Introduced source (b) Obtained and introduced density

Figure G.2: Theoretical source and density

The following are the estimation results for the parameters (fig.G.3) and the tracked density normalized error (fig.G.4)

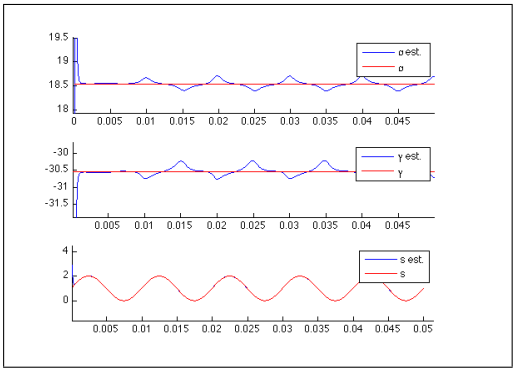

Figure G.3: Estimated and real parameters

It can be observed that, after a short initial time, the estimated parameters keep to follow the real parameters with a small error. Also the modulation of the source is well estimated.

Regarding the normalized density error, we can observe that the estimated density follows the theoretical one with an error such that

$$\epsilon(t) = \frac{||n(t) - \hat{n(t)}||_2^2}{||n(t)||_2^2} \sim 10^{-9}$$

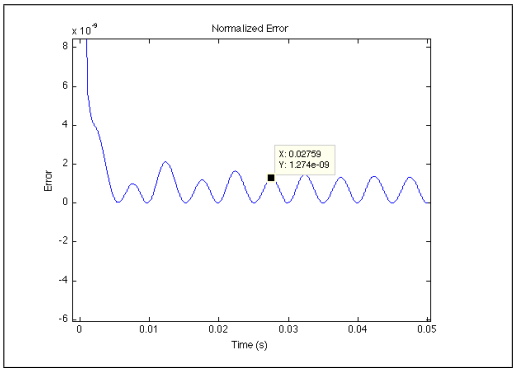

Figure G.4: Normalized estimation error

Appendix H

Tore supra data shots used during the project

The data measurements obtained from the Tore Supra experiences is what we know as data shots. This experiences are carried out under previously determined conditions (Heat sources, plasma current, magnetic field, plasma position...). The data shots from this experiences can be obtained using different codes accessing the Tore Supra database. To distinguish one data shot, it is designated by a number after the TS abbreviation. In this project, several data shots has been used; here we explain the two main data shots appearing in this project: The TS38953 and TS45525.

A The TS38953 data shot

The TS38953 data shot was obtained from an experience in which the power emitted by the LH antenna had been modulated and the plasma current had been set in three different values: 0.6 MA, 0.5 MA, and 0.3 MA. For this experience, the antenna protection limiter (LPA) had been taken off so that no other source apart from the LH antenna source and the toroidal limiter source appeared.

The position of the plasma facing components for this shot were:

- LPT: $R_{mean} = 3.1$ m
- LH: $R = 3.156$ m

The following graphs show the configuration values for the experience and the density distribution.

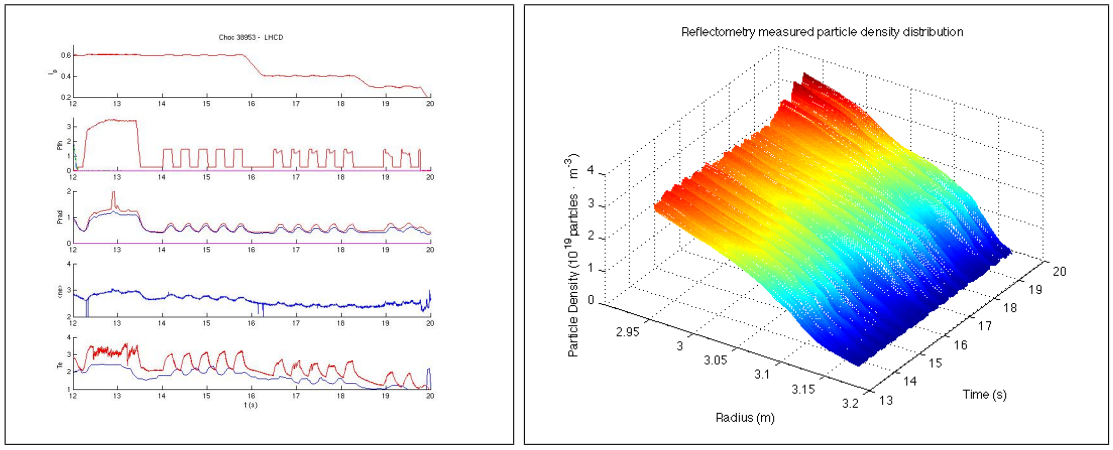

(a) Characteristic values for the experience (b) Density distribution

Figure H.1: Data shot TS38953

B The TS45525 data shot

The TS45525 data shot was obtained from an experience where the LH antenna was constantly powered. Since the plasma current was also constant, the density distribution only suffers small variation due to perturbations and its own turbulences. In this experience, the LPA was installed.

The position of the plasma facing components for this shot were:

- LPT: $R = 3.086$ m
- LPA: $R = 3.116$ m
- LH: $R = 3.153$ m

In the following figures the characteristics of the shot and the density distribution are shown.

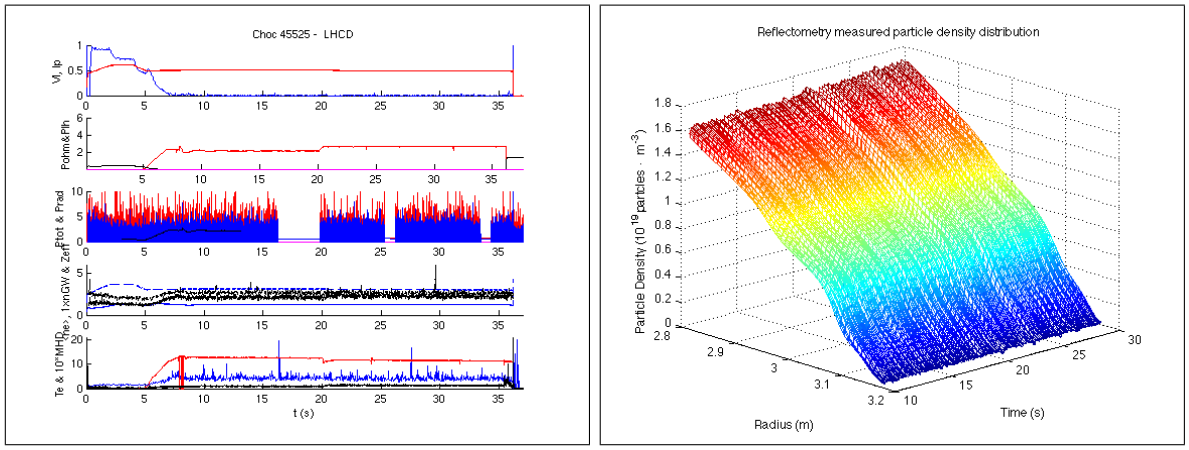

(a) Characteristic values for the experience (b) Density distribution

Figure H.2: Data shot TS45525

Bibliography

[1] International Energy Agency, *"Key World energy statistics"*, pub. 2009.

[2] International Energy Agency, *"World Energy Outlook"*, pub. 2008.

[3] Jerome C. Glenn, Theodore J. Gordon, and Elizabeth Florescu, *"State of the Future"*, pub. 2009.

[4] World Health Organization, *"Report of the UN Chernobyl forum"*, 2006.

[5] J. Adam, *"La fusion nucléaire: Une source d'énergie pour l'avenir?"*

[6] E. Witrant, M. Goniche and Equipe Tore Supra, *"A QSS approach for particle source identification in Tore Supra tokamak"*, Proc. of 48th IEEE Conference on Decision and Control, Shanghai, December 16-18, 2009. Invited paper.

[7] J. Weydert, E. Wittrant, M. Goniche, *"Source determination in non-homogeneous dissipative media*, M2 report, 2009.

[8] A. Ekedahl, G. Granucci, J. Mailloux, Y. Baranov, S.K. Erents, E. Joffrin, X. Litaudon, A. Loarte, P.J. Lomas, D.C. McDonald, V. Petrzilka, K. Rantamaki, F.G. Rimini, C. Silva, M. Stamp, A.A. Tuccillo and JET EFDA Contributors *"Long distance coupling of lower hybrid waves in JET plasmas with edge and core transport barriers"*

[9] G.F. Matthews et al., *"The effect of CD_4 puffing on the peripheral scrape-off layer in JET"*

[10] J. Miles, M. Fikar, *"Process Modelling, Identification and Control", Ch.8*, in Springer (Ed).

[11] J. Moret and Equipe Tore Supra, *"Tokamak transport phenomenology and plasma dynamic response"*, Nucl. Fusion, vol.32, no 7, pp. 1241-1258, 1992.

[12] Garbet Association Euratom-CEA, CEA/DSM/DRFC CEA-Cadarache, *"Plasma Edge physics"* France Master Sciences de la Fusion October,6 2008.

[13] M. Kican, J. Gunn, J. Y. Pascal, G. Bonhomme, C. Fenzi, E. Gauthier and J. L. Segui, *"Edge ion-to-electron temperature ratio in the tore supra tokamak"*, Plasma Phys. Control. Fusion, vol 50, pp. 125009 - 125019, 2008.

[14] E. Witrant and Nicolas Marchand, *'Modeling and feedback control for air flow regulation in deep pits"*